Full title: **Planar polarization of cilia in the zebrafish floor-plate involves Par3-mediated posterior localization of highly motile basal bodies**

Short title: **Par3 controls cilia posterior positioning in zebrafish floor plate**

Antoine Donati[1], Sylvie Schneider-Maunoury[1*] and Christine Vesque[1*]

[1] Sorbonne Université, CNRS UMR7622, INSERM U1156, Institut de Biologie Paris Seine (IBPS) - Developmental Biology Unit, 75005, Paris, France

*co-senior authors, co-corresponding authors.

sylvie.schneider-maunoury@upmc.fr 0144272154

christine.vesque@upmc.fr 0144272154

Keywords: planar cell polarity, cilium, basal body, zebrafish floor plate, Par3, Vangl2.

Non-standard abbreviations:

BB: basal body (a modified centriole localized at the base of cilia)

FP: floor plate (a multi-functional epithelium localized at the ventral side of the neural tube. Floor plate motile cilia generate the cerebro-spinal fluid directional flow)

ABSTRACT

To produce a directional flow, ciliated epithelia display a uniform orientation of ciliary beating. Oriented beating requires planar cell polarity (PCP), which leads to planar orientation and asymmetric positioning of the ciliary basal body (BB) along the polarity axis. We took advantage of the polarized mono-ciliated epithelium of the embryonic zebrafish floor plate to investigate by live-imaging the dynamics and mechanisms of BB polarization. We showed that BBs, although bearing a cilium, were highly motile along the antero-posterior axis. BBs contacted both the anterior and the posterior membranes, with a bias towards posterior contacts from early somitogenesis on. Contacts exclusively occurred at junctional Par3 local enrichments or “patches” and were often preceded by transient membrane digitations extending towards the BB, suggesting focused cortical pulling forces. Accordingly, BBs and Par3 patches were linked by dynamic microtubules. We showed that Par3 became posteriorly enriched prior to BB posterior positioning and that floor plate polarization was impaired upon Par3 patches disruption triggered by Par3 or aPKC overexpression. In the PCP mutant *Vangl2*, where floor plate cells fail to polarize, we observed that BB were still motile but presented behavioral defects, such as ectopic contacts with lateral membranes that correlated with Par3 patch fragmentation and spreading to lateral membranes. Our data lead us to propose an unexpected function for posterior local Par3 enrichment in controlling BB asymmetric positioning downstream of the PCP pathway via a microtubule capture/shrinkage mechanism.

72 INTRODUCTION

73

74 Cilia are conserved microtubule-based organelles with sensory and motile functions
75 that are nucleated from a modified centriole called the basal body (BB). Motile cilia
76 generate forces sufficient to propel whole organisms or bodily fluids within cavities in
77 animals ([1],[2]). In order to generate a directional flow, ciliated epithelia display a
78 uniform orientation of ciliary beating, which is a form of planar cell polarity (PCP).
79 Oriented beating of a cilium usually involves two PCP processes: the off-centering of
80 the cilium BB (translational polarity, in monociliated epithelia and ependymal cells)
81 and the orientation of its beating relative to the main tissue axis (rotational polarity)
82 ([1]).

83 In many vertebrate ciliated tissues such as the mouse cochlea and ependyma, the
84 laterality organ of mouse and zebrafish, the Xenopus larval skin and the zebrafish
85 floor plate, cilium polarity requires the PCP pathway. In these tissues, PCP proteins
86 such as Van Gogh like 2 (Vangl2), Frizzled (Fz3/6), Cadherin EGF LAG seven-pass
87 G-type receptors (Celsr1-3) and Dishevelled (Dvl1-3), localize asymmetrically in
88 ciliated epithelia, and are required for proper cilia/BB positioning ([3], [4], [5], [6], [7], [8]).
89 Outside the PCP pathway, the cellular and molecular mechanisms of BB positioning
90 remain poorly understood. Non-muscle myosin II is required for ependymal
91 translational polarity in murine ependymal multiciliated cells ([9]) and the murine
92 Myosin Id mutant exhibit defects in both translational and rotational polarity in these
93 cells ([10]). Translational polarity has been shown to require Rac1 in monociliated cells
94 of the mouse node and cochlea ([11],[12]) and G protein signalling in cochlear hair cells
95 ([13], [14]). Ciliary proteins themselves have been involved in planar polarization of cilia in

96 several contexts ([6], [15], [16], [17], [18]). However, the relationships between these different
97 actors and how they impact basal body movement is unclear.

98 Understanding the mechanisms of cilium polarization would highly benefit from a
99 dynamic analysis of BB movements. A major drawback is the difficulty to follow the
100 dynamics of BB polarization *in vivo* in whole embryos, or to reproduce PCP and
101 cilium polarization *in vitro* in cultured cells. So far, live imaging of cilium polarization
102 has been performed only in cochlear explants where only confined Brownian motion
103 of centrioles was observed ([19]) and in the mouse node ([11]) and ependyma ([9]) with
104 limited temporal resolution. In this paper, in order to get a better understanding of the
105 mechanisms leading to BB off-centering in epithelia, we have used the zebrafish
106 embryonic floor-plate (FP) as a convenient system to investigate the dynamics of the
107 polarization process in live embryos. The FP is a simple mono-ciliated epithelium
108 whose posterior-positioned motile cilia allow circulation of the embryonic
109 cerebrospinal fluid ([20]).

110 Our results show that planar polarization of BBs and their associated cilia is
111 progressive during somitogenesis and is accompanied by a change in the behavior of
112 the BBs, which are highly motile at early stages and tend to spend an increasing
113 amount of time in contact with the posterior membrane as development proceeds.
114 We found that BBs always contacted membranes at Par3-enriched apical junctions.
115 Par3 became enriched at the posterior apical side of FP cells before BB polarization.
116 Par3 and aPKC overexpression disrupted FP polarization and Par3 distribution along
117 apical junctions was also disrupted in a *Vangl2* mutant. Thus, we propose that a
118 major role of the PCP pathway in the FP is to drive Par3 asymmetric localization,
119 which in turn mediates BB posterior positioning.

120 RESULTS

121

122 Floor-plate polarization shows temporal progression but no spatial
123 synchronization

124 Posterior positioning of the BB in the zebrafish FP is visible as soon as 18 hours
125 post-fertilization (hpf) ([17]) and is maintained at least until 72 hpf ([21]). From 24 hpf
126 onward, coupled to posterior tilting of cilia, it is instrumental in propelling the
127 cerebrospinal fluid in the spinal cord central canal ([5,22]). At late gastrulation stages
128 (10 hpf), ectodermal cells already display a slight posterior bias of centrioles ([23]).

129 To define the time-course of FP cell polarization, we assessed basal-body (BB)
130 position along the antero-posterior (A/P) axis on fixed embryos from the 6 s to the 26
131 s stage ("s" stands for "somites")(Fig. 1b, c). For each cell we defined a BB
132 polarization index (p.i. in Fig. 1a). BBs already exhibited a posterior bias at 6 s, and
133 the polarization state did not change significantly until 10 s. From 10 s onward, there
134 was a progressive increase in FP polarization, mostly due to an increase in the
135 percentage of cells with a BB in contact with the posterior membrane, with a
136 concomitant disappearance of anterior BBs and a reduction of median BBs. The
137 polarization state of the FP was considered complete at 18 s, since no significant
138 difference could be detected between the 18 s and 26 s stages (Fig. 1c).
139 Interestingly, we did not detect a gradient of polarization index along the A/P axis of
140 the spinal cord (Fig. S1a), and single non-polarized cells were often intermingled
141 among polarized neighbors (Fig. S1b), arguing against the existence of polarization
142 waves.

143 **BBs are highly motile in FP cells**

144 We then turned to live-imaging to obtain a dynamic view of the polarization process.
145 We followed BB movements within the apical surface of individual FP cells at
146 different developmental stages (4 s to 21 s). We found that BBs displayed a highly
147 motile behavior within the apical surface (Fig. 2a-d and Movies S1-S4), moving both
148 anteriorly and posteriorly (Fig. S1d, first column and Fig. 6a 'wt'). At early stages,
149 there was a clear BB movement orientation bias along the antero-posterior axis: 70%
150 of BB movements were oriented along this axis, whereas only 30% were oriented
151 along the left-right axis (Fig. 6a, b, wt). However there was no overall significant
152 difference between the number of anterior and posterior movements (although there
153 seems to be a tendency towards more posterior movements, as seen in Fig. 6a).

154 Cell deformations along the AP axis were more important at early stages (4-10 s)
155 (Fig. 2a, b) than at later stages (14-21 s) (Fig. 2c, d), probably as a consequence of
156 convergence-extension movements, but even at early stages we could see many
157 long BB movements that did not correlate with cell deformation (see for example the
158 two large anterior and then posterior movements around 55 and 75 min in Fig. 2a).
159 This suggest that BBs are actively moving within FP cell apical surfaces and not just
160 passively moved by cell deformation. One possible explanation for the presence of
161 unpolarized cells is that they could have just undergone mitosis (during which one of
162 the centrosomes migrates to the anterior side). However, mitoses were rare in FP
163 cells at early stages (6 / 79 cells, 9 embryos at 4-8 s) and absent at later stages (118
164 cells from 15 embryos at 13-21s). Thus the impact of cell shape changes and mitosis
165 on FP polarization is likely very small.

166 **FP polarization involves a change in BB behavior**

167 In order to characterize BB behavioral changes during development, we determined
168 the percentage of time that BBs spent in contact with the posterior membrane (Fig.
169 2e). At early stages, BBs spent in average 44% of their time in contact with the
170 posterior membrane, versus more than 70% at later stages (13-21 s). This was
171 largely due to an increase in the number of cells in which the BB stayed in contact
172 with the posterior membrane during the whole movie (Fig. 2c). We refer to this
173 situation as “posteriorly docked BB”. At early stages (4-8s), we did not observe any
174 cell with posteriorly docked BB (41 cells, 5 embryos), whereas they made up 34% of
175 the FP cell population at 13-17s stages (13/38 cells, 6 embryos) and almost half
176 (46%) the FP population at later stages (17-21s, 27/59 cells, 7 embryos). We also
177 noted a decrease in the frequency of BB direction changes, as well as an increase in
178 the mean duration of BB/posterior membrane contact events and mean polarization
179 index, suggesting that, as development proceeds, BB movements are less dynamic
180 and more confined to the posterior side of the cell (Fig. S1d, first line). Posteriorly
181 docked BBs made a significant contribution to these behavioral changes. In order to
182 determine if changes in the behavior of non-posteriorly docked BBs contributed to the
183 increase of FP polarization during somitogenesis, we quantified the same
184 parameters, but taking into account only these motile BBs (Fig. S1d, second line):
185 although less drastic, the same trend in BB behavior change was observed.

186 To further characterize the behavior of non-posteriorly docked BB, we quantified the
187 frequency of contact events between the BB and either the anterior or the posterior
188 membrane (Fig. 2f and g, respectively). First, posterior contacts were more frequent
189 than anterior ones even at 4-8s (compare Fig. 2f and g), confirming that FP cells
190 already had a posterior polarization bias at these early stages. Second, contacts with

191 the anterior membrane were frequently observed at early stages (50% of BBs made
192 at least one anterior contact per hour, see for example at t=70' in Fig. 2b), but almost
193 never observed at later stages (only 3/57 cells displayed one anterior contact).
194 Contact frequency with the posterior membrane was also significantly higher at
195 earlier stages (1.3 contact/h on average) than at later stages (around 0.8
196 contact/hour in average within the 13-21s stage window, Fig. 2g). This reduction in
197 the number of contacts could be due to an increase in their duration (Fig. S1d, plot
198 2nd column, 2nd line) and to a reduction in BB speed. Indeed, we found that BBs
199 moved faster at earlier stages (Fig. S1c, median speed was 0.2 μm/min at 4-8 s
200 versus 0.1 μm/min at 13-21 s). Thus, the observed changes in FP polarization are
201 explained both by an increase in the posteriorly docked BB population and by
202 behavioral changes (reduced speed, less direction changes, longer posterior contact
203 events) in other BBs.

204 Transverse membrane digitations elongate towards motile floor-plate 205 BBs

206 Live-imaging revealed the presence of membrane digitations extending between the
207 BB and transverse membranes (Fig. 3; Movies S5 and S6). At early stages, we could
208 detect such digitations in 44% of FP cells (taking into account only non-posteriorly
209 docked BBs) (26/59 cells, 9 embryos), most of which were linking the posterior
210 membrane and the BB (83%, 45/54 digitations, Fig. 3a upper row, white arrow,
211 MovieS5), although digitations from the anterior membrane were also seen (Fig. 3a
212 second row, Movie S6) (Fig. 3b). These early stage digitations were most of the time
213 observed on a single time frame (anterior digitations) or two consecutive timeframes
214 in time-lapse movies with a 2min or 5min time interval (Δt2min or Δt5min,

215 respectively) between two images, but we could not detect a significant difference of
216 digitation lifetime between anterior and posterior digitations (Fig. 3c). Posterior
217 digitations were followed by a posterior directed BB movement in 67% of cases
218 (26/39 digitations), whereas anterior digitations were followed by a BB anterior
219 movement in only 22% of cases (2/9 anterior digitations) (Fig. 3d). Membrane
220 digitations were rarely seen at later stages (after 14s, 9/40 cells, 10 embryos),
221 probably in part because BBs spent a higher fraction of their time associated with the
222 posterior membrane (see Fig. 1 and Fig. S1).

223 In order to better characterize these membrane digitations at early developmental
224 stages, we imaged the floor-plate of wt embryos at a high temporal resolution and
225 acquired a z-stack every 10 seconds (hereafter, Δt10sec movies). Digitations were
226 seen in 80% of FP cells (25/31 cells from 17 embryos), showing that these structures
227 are very common in FP cells but can be missed in Δt2min or Δt5min movies due to
228 their short lifetime. Indeed, we found that digitations had a median lifetime of 50sec
229 (FigS2b). In many cases, we could witness both digitation extension and retraction.
230 Their median length at their maximal extension was 2μm (Fig. S2b) and almost all
231 digitations pointed towards the BB (95%, 90/95 digitations, 25 cells from 14 embryos)
232 and about 45% of them touched the BB. As previously mentioned, almost all
233 digitations extended from transverse membranes (92%, 88/95, FigS2a) and most
234 digitations formed at a spot were we could previously see another digitation
235 ("recurrent" digitations, 85%, 44/52); the median time lapse between two successive
236 digitations was 70sec (Fig. S2b). As with our Δt2min and Δt5min movies, there was
237 not a good correlation between digitation position (anterior or posterior membrane)
238 and BB movements: posterior digitations were followed by a posteriorward BB

239 movement in 40% of cases (16/40) whereas anterior digitations were followed by an
240 anteriorward BB movement in only 30% of cases (13/34) (Fig. S2c) suggesting that
241 these digitations are not responsible for BB movements but rather a consequence of
242 the forces exerted on BBs.

243 **Dynamic microtubules link BBs and transverse membranes**

244 Since centrosomes are the main microtubule organizing centers of animal cells and
245 their positioning in many systems has been shown to depend on microtubules we
246 then set out to investigate microtubule dynamics within the apical surface of FP cells
247 in early stage embryos. Live-imaging of microtubules with EB3-GFP revealed a highly
248 dynamic network of microtubules originating from the centrosome/BB and directed to
249 apical junctions (FigS2d, Movie S7). The time interval between an EB3 comet coming
250 from the BB touching a spot at the transverse membrane and the occurrence of
251 either a digitation at this spot or a BB movement towards it was very short: 10 sec in
252 50% of the cases and less than 1 min in 95% of the cases (Fig. S2e). These results
253 show the existence of dynamic microtubules linking the BB and particular spots of the
254 apical transverse membranes before BB movement toward these spots and/or
255 digitation formation at these spots. This suggests that the mechanical forces
256 responsible for the back-and-forth BB movements between the anterior and posterior
257 transverse membranes are mediated by dynamic microtubules.

258 Overall, our dynamic analysis reveals a highly motile behavior of BBs in FP cells at
259 early somite stages. This was unexpected, given that FP cells are already ciliated at
260 these stages (Fig. 1b) ([5]). As somitogenesis proceeds, BB motility decreases. BBs
261 progressively stop shuttling from anterior to posterior cell junctions and their contacts
262 with the posterior membrane last longer. We also uncover membrane digitations

263 forming at precise spots of transverse apical membranes and show that these spots
264 are linked to BBs by dynamic microtubules. These results suggest the existence of a
265 molecular complex at precise spots of transverse membranes, probably at the level
266 of apical junctions, which is able to exert mechanical forces on the BB via
267 microtubules, and whose distribution becomes biased to the posterior side of each
268 FP cell as development proceeds.

269 **Posterior enrichment of Par3 precedes BB/posterior membrane contact**

270 In Drosophila, the apical junction protein Par3/Bazooka modulates centrosome
271 positioning in the male germline and embryonic ectoderm ([24],[25]). In order to test a
272 potential role for Par3 in BB posterior positioning in FP cells, we first assessed Par3
273 localization by immunostaining (Fig. 4a). At the 14 s stage, Par3 localized at apical
274 junctions of FP cells (Fig. 4a). Par3 patches were detected on transverse membranes
275 and in close contact with posteriorly docked BBs (white arrows, Fig. 4a). This
276 distribution was confirmed using the BazP1085 antibody (Fig. S3a), which recognizes
277 a conserved Par3 phosphorylation site ([26]). Par3 patches were also present in FP
278 cells in which the BB was not yet in contact with the posterior membrane (Fig. 4a and
279 S3a right panels) showing that this enrichment precedes stable BB/posterior
280 membrane contact.

281 In order to test whether Par3 is asymmetrically enriched in FP cells, we used a
282 mosaic expression approach of Par3-RFP and centrin-GFP in live embryos.
283 Quantification of Par3 expression showed that, among fully polarized (p.i. =1)
284 individual Par3-RFP expressing FP cells, both at early (6-12s, Fig. 4b, left cell) and
285 late (14-20s, Fig. 4b, right cell) stages, almost all cells had a Par3-RFP post/ant ratio
286 greater than 1 (Fig. 4b right plot) (29/30 cells, 20 embryos; 6-12s, mean ratio= 1.42,

287 14-20s mean ratio =1.38). To determine whether Par3 posterior enrichment preceded
288 BB/posterior membrane contact, we imaged BB movements and quantified Par3-RFP
289 posterior/anterior ratio at each time-point; we found that Par3-RFP was enriched
290 posteriorly before BB/posterior membrane contact (Fig. 4c, d) (12/14 cells, 12
291 embryos) (Movie S8). In contrast, BBs of FP cells with weak or no posterior Par3
292 enrichment remained unpolarized (either making no contact (2/5 cells, 5 embryos) or
293 unstable contacts (3/5 cells, 5 embryos) with the posterior membrane (Fig. 4d and
294 Movie S9).

295 Thus, Par3 forms patches at FP apical transverse membranes and BBs are
296 posteriorly docked at these patches. In addition, Par3 is enriched posteriorly before
297 BB/posterior membrane contact. Together, our data strongly suggest that Par3 is a
298 key player in BB posterior positioning.

299 At early stages, BBs contact transverse membranes exclusively at Par3 300 patches

301 During the second half of somitogenesis, Par3 formed a continuous belt at apical
302 junctions of FP cells, although it was locally enriched, forming patches that
303 associated with centrosomes, as described above. In contrast, at the 4 to 8 s stages,
304 Par3 formed discrete patches at FP apical transverse membranes, but not at lateral
305 membranes. These patches were roughly aligned with the AP axis of the embryo
306 (Fig. 4e, white arrows). Strikingly, BBs made contacts with anterior and posterior
307 transverse membranes (as described in Fig. 1) exclusively at these patches (58 cells
308 from 18 embryos) as shown in Fig. 4f and Movies S10 and S11.

309 In 40% of these cells (23/58), the discrete Par3 patches stretched towards the BB
310 (for example, Fig. 4f yellow arrows) and was actually covering a membrane digitation
311 originating from either the posterior (Fig. 4f, t=0', see also inset on the right) or the
312 anterior membrane (Fig. 4f, t=64') and extending towards the BB (Movie S11). Of the
313 39 digitations we saw, 92% were located at a Par3 patch (36/39 digitations from 23
314 cells and 14 embryos)(see Movie S11 at t=32min for a rare example of a digitation
315 not originating at a Par3 patch). The presence of membrane digitations and their
316 overlap with Par3 patches point to the existence of mechanical forces between BBs
317 and membranes at Par3 patches and suggests that Par3 could be required for local
318 force generation. Strinkingly, this role of Par3 could be more general than just BB
319 antero-posterior contacts, since in dividing FP cells at early stages, after cytokinesis
320 the centrosomes always rapidly (within 10min) moved back towards Par3 patches,
321 next to the midbody (9/9 cells from 9 embryos, Fig. S3b and Movie S12).

322 Par3 over-expression or aPKC-mediated clustering defects disrupt BB 323 positioning

324 To test whether Par3 is required for posterior BB positioning in the FP, we first used
325 loss-of-function approaches. MO-mediated knock-down of Par3ab (also known as
326 Pard3 or ASIP) did not disrupt FP PCP (Fig. S4a), nor could we see a defect in a
327 *MZpar3ab* mutant ([27]) (Fig. S4c). However, in both cases, Par3 patches could still be
328 detected in the FP by immunostaining (Fig. S4b, d-f), suggesting that *par3ab* loss-of-
329 function was compensated for by its paralogous genes (*par3aa*, *par3ba* or *par3bb*),
330 which could also be detected by our Par3 antibodies thanks to the high conservation
331 of the epitopes. In situ hybridization for all *par3* genes showed that *par3aa*, *ab* and *ba*
332 were broadly expressed in the neural tube during somitogenesis (Fig. S5a).

333 Combining MOs against these three genes did not lead to FP polarization defects,
334 but Par3 patches were still present and their prominence and number not affected,
335 despite a significant loss in Par3 immunostaining signal (Fig. S5b-f): we could not test
336 the effect of higher doses of MOs on FP polarization due to a developmental arrest
337 before somitogenesis.

338 We thus turned to a mild over-expression approach to disrupt Par3 posterior
339 enrichment and patch formation. Over-expressed Par3-RFP in the FP localized to
340 apical junctions and did not disrupt apico-basal polarity (Fig.5a). Par3-RFP over-
341 expression disrupted BB posterior positioning in the FP (median p.i. of 0.8 versus 1 in
342 Par3-RFP negative cells, Fig. 5a,). Furthermore, isolated Par3-RFP negative cells
343 and Par3-RFP negative cells adjacent to Par3-RFP over-expressing cells had similar
344 polarization indexes, showing that Par3 overexpression effect is cell autonomous
345 (147 isolated negative cells and 391 non-isolated negative cells from 20 embryos,
346 Wilcoxon test p-value=0.19).

347 In order to confirm these results, we used another approach to disrupt Par3
348 endogenous distribution via aPKC over-expression ([25],[28]). We found that mosaically
349 over-expressing aPKC with the KalTA4-UAS system (a Zebrafish-optimized GAL4-
350 UAS system[29]) led to BB polarization defects similar to Par3 overexpression (Fig.
351 5b). In addition, in these experiments, the extent of Par3 localization defects
352 correlated with that of BB polarization defects. In one experiment where we observed
353 a significant decrease in Par3 patch prominence in aPKC overexpressing cells, we
354 also observed a significant decrease in BB polarization (Fig. 5d, "experiment 1"). In
355 another experiment where the change in Par3 patches prominence was present but
356 not statistically significant, BB positioning was less affected (Fig. 5d, "experiment 2").

357 Together, these results indicate that the extent to which the polarization is affected
358 indeed depends on the strength of the effect on Par3 patches.

359 These results strongly suggest that Par3 posterior enrichment and patch formation
360 are required for proper BB positioning in the FP.

361 In the PCP mutant *vangl2* BB are still motile but make more contacts
362 with lateral membranes

363 Vangl2, a core PCP protein, is involved in zebrafish FP PCP ([5]) but the downstream
364 mechanisms linking Vangl2 to centrosome posterior positioning are unknown. We
365 thus analyzed the dynamics of FP polarization in the *vangl2*^{m209} mutant ([30]). At 18 s,
366 the BB of *vangl2*$^{m209/m209}$ FP cells was mispositioned at the center of the apical
367 surface, while *vangl2*$^{m209/+}$ and wt embryos had normally polarized BBs (median
368 p.i.=0.6 versus 1 for wt or *vangl2*$^{m209/+}$) (Fig. 7a, FP polarization plot). Live-imaging of
369 *vangl2*$^{m209/m209}$ FP revealed several BB behavior changes in *vangl2*$^{m209/m209}$.

370 At early stages in *vangl2*$^{m209/m209}$ FP cells, BBs were still motile and even displayed
371 an overall speed increase (Fig. 6d). Moreover, BB movements were still biased along
372 the antero-posterior axis (Fig6b, 60% of total BB movements; 9 embryos, 20 cells,
373 220 movements), but BBs made more lateral movements and less antero-posterior
374 movements compared to wt (10% less antero-posterior movements, Fig. 6a and 6b,
375 Movie S13). The length of BB movements, which was smaller in the lateral than in
376 the antero-posterior direction in wt, was equivalent in all directions in *vangl2*$^{m209/m209}$
377 mutants (Fig. 6a).

378 Despite the preserved antero-posterior bias in BB movements, *vangl2* mutants
379 showed a striking loss of antero-posterior bias in BB/membrane contacts. The overall

380 proportion of BB movements resulting in BB/membrane contacts was the same as in
381 wt (around 16% of total BB movements), but the positions of these contacts were
382 very different: in wt, most contacts occurred with the posterior membrane (75%) and
383 almost none with the lateral membranes (3%), whereas in *vangl2*$^{m209/m209}$, BB
384 contacts occurred equally with anterior, posterior or lateral membranes (around 33%
385 each) (Fig. 6d, middle barplot). In addition, *vangl2*$^{m209/m209}$ BBs spent less of their
386 time in contact with either anterior, posterior and lateral membranes (Fig. 6d, right
387 plot).

388 At later stages, almost half of the BBs remained in contact with the posterior
389 membrane in wt, as previously described (Fig. 2e) (posteriorly docked BBs). In
390 *vangl2*$^{m209/m209}$ embryos, the vast majority of BBs did not stably dock at any
391 membrane (except for 2 BB out of 42, docked at the anterior membrane). Instead, as
392 suggested by our immunostaining, BBs remained at the center of the apical surface.
393 The few BB movements of wt cells as well as the many BB movements seen in
394 *vangl2*$^{m209/m209}$ cells were much smaller than at early stages (which is illustrated by a
395 decrease in BB speed (Fig. 6e)) and had no preferential orientation (Fig. 6a).
396 BB/membrane contacts were half less frequent than at early stages, both in wt and
397 *vangl2*$^{m209/m209}$ (around 7% of total BB movements), but we could still detect a
398 significant difference in their position between wt and *vangl2*$^{m209/m209}$, with more
399 lateral and anterior contacts in *vangl2*$^{m209/m209}$ (Fig. 6e, middle barplot).

400 **BB behavior defects in *vangl2* mutants are associated with abnormal**
401 **Par3 clustering and localization**

402 Since in wt embryos BBs only made contacts at Par3 patches, we wondered if it
403 would still be the case in *vangl2* mutants. Par3 localized at apical junctions in

404 *vangl2*$^{m209/m209}$ as in wt embryos (Fig. 7b). However, quantification of Par3 patches
405 along the transverse apical junctions revealed a significant difference in the number
406 and prominence of these patches. In wt, 90% of FP cells had at least a major Par3
407 patch (Fig. 7b, yellow arrows), with 39% of cells also having smaller secondary
408 patches (Fig. 7c), while in *vangl2*$^{m209/m209}$ embryos, the number of FP cells with at
409 least one phospho-Par3 patch was unchanged (around 90% of cells) but the number
410 of cells with more than one patch was increased (54% of cells). In addition, the
411 prominence of phospho-Par3 patches fluorescence intensity was decreased in
412 *vangl2*$^{m209/m209}$ embryos (see Fig. 5c for prominence definition and quantification).
413 Thus, Par3 forms more numerous and smaller patches in *Vangl2* mutants, showing a
414 role for Vangl2 in Par3 clustering.

415 To further analyze a potential link between abnormal BB behavior and Par3 patches
416 mis-localization in *vangl2*$^{m209/m209}$ embryos, we made time-lapse movies of mutant
417 embryos mosaically injected with Par3-RFP (Fig. 7f) (Movie S13). In *vangl2* mutants,
418 FP cell BBs contacted the membrane only at Par3 patches (Fig. 7e), as seen in wt,
419 suggesting that Vangl2 did not directly affects the ability of Par3 patches to attract
420 BBs. However the distribution of Par3 patches was very different. Early
421 *vangl2*$^{m209/m209}$ embryos displayed many more cells with lateral Par3 patches
422 compared to wt (70% vs 20%, Fig. 7g). In addition, they had more cells with an
423 anterior Par3 patch (82% vs 67%) and less cells with a posterior patch (65% vs
424 87%).

425 These results strongly suggest that, in *vangl2*$^{m209/m209}$ embryos, abnormal BB
426 behavior and polarization failure are due to the fragmentation and mispositioning of
427 Par3 patches along the apical junctions of FP cells.

428 DISCUSSION

429 In this paper we have analyzed the dynamics of BB posterior positioning in the
430 embryonic zebrafish FP. We show that, during early somitogenesis, BBs are highly
431 motile and able to contact apical junctions several times per hour. As somitogenesis
432 proceeds, BBs settle down posteriorly at junctions enriched in Par3, and we show
433 that Par3 enrichment is essential for BB posterior localization. In the PCP mutant
434 *Vangl2*, BBs show poorly oriented movements and this correlates with Par3 signal
435 fragmentation and spreading to lateral junctions (Fig. 8a). Our data lead us to
436 propose a model in which Par3 posterior enrichment, controlled by the core PCP
437 pathway, increases microtubule-driven pulling forces from the posterior side, which
438 eventually results in BB docking at the posterior Par3 patch (Fig.8b).

439 ***Ciliary basal bodies exhibit high motility in FP cells of wt and vangl2***
440 ***mutant embryos***

441 Analysis of fixed samples showed that posterior positioning of BBs within the apical
442 surface of FP cells progressed regularly within the 8 hours time frame of our study
443 and was complete at the 18 s stage. Surprisingly, live imaging revealed that BBs
444 make fast back and forth movements within the apical surface. This high motility of
445 the BB (median speed 0.2 μ/min at 4-8s) is unexpected given the presence of a
446 growing cilium anchored to its distal part. It contrasts with the situation in the mouse
447 cochlea, where live-imaging of explants have suggested very slow and regular
448 movements of the BBs to the lateral cortex of inner hair cells (estimated speed of 10-
449 50 nm/h) ([19]). BB motility decreases at later stages of polarization, coincident with
450 their posterior docking. Live imaging also uncovered a clear antero-posterior bias in
451 BB movements, indicating that the orientation of the forces underlying these

452 movements is biased along the polarization axis from early stages on. However, we
453 could not detect a significant global posteriorward bias in these movements in early-
454 stages FP cells (Fig. 6a).

455 In fixed samples of *vangl2* mutants, the BBs remain at the center of the FP cell apical
456 surfaces ([5] and Fig. 7a-b), suggesting a decrease in their motility. Strikingly, our
457 dynamic analysis revealed that in *vangl2*$^{m209/m209}$ embryos, BBs are still highly motile.
458 Major differences with wt BBs are that they make many contacts with lateral
459 membranes, whereas wt BBs do not, and that their contacts are shorter than for wt
460 BBs. This suggests that there are molecular cues at the membrane organizing/driving
461 BB movements, and that these cues are still present but disorganized in space in
462 PCP mutants.

463 Thus, our live imaging study uncovers a totally unexpected motile behavior of BBs
464 during a cilia planar polarization process. It will be interesting to investigate whether
465 this behavior is conserved in other tissues undergoing cilia translational polarity.

466 ***Par3 cortical patches recruit the BB.***

467 We proposed the asymmetric maturation of cell junctions as a possible cause for
468 posterior BB positioning. Accordingly, we found that Par3 accumulated in patches at
469 the posterior apical junctions of FP cells before BB posterior docking. Moreover, we
470 showed that perturbed Par3 localization affected BB polarization. Interestingly, in the
471 Drosophila early gastrula ectoderm, Par3 isotropic distribution around apical junctions
472 contributes to epithelial integrity, but in aPKC loss of function mutants, Par3
473 accumulates as discrete patches that align along the dorso-ventral axis and "recruit"
474 centrosomes ([25]). Centrosome docking at discrete Par3 patches has also been

475 observed in Drosophila germ stem cells and is critical for proper division orientation
476 ([24]). Together with these published data, our results on BB positioning in zebrafish FP
477 strongly suggest that Par3 may be broadly involved in recruitment of centrosomes
478 and BBs in different systems.

479 Our live imaging data strongly suggest that Par3 is involved in generating mechanical
480 forces on BBs to pull it toward the membrane. First, the BB contacts the membrane
481 exclusively at Par3 patches. Second, membrane deformations support the existence
482 of mechanical forces between Par3 patches and BBs. Third, the predominance of
483 posterior digitations over anterior ones (Fig. 3b) suggests that more force is exerted
484 on the BB from the posterior side, where Par3 is enriched. Such membrane
485 digitations have been previously observed during cell division in the *C. elegans*
486 zygote ([31]), in the *C. intestinalis* embryo ectoderm ([32]) and in rare cases at the
487 immunological synapse ([33]). In all cases, the existence of pulling forces between the
488 centriole and the membrane has been proposed.

489 We propose that digitations are a consequence of mechanical forces between the BB
490 and Par3 patches rather than a driver of BB movement (as was previously
491 hypothesized in Ciona embryos ([32])). First, digitations were rare (even in Δt10sec
492 movies, only half of BB movements were associated with digitations) and second,
493 there was not a good correlation between the location of a digitation and the direction
494 of BB movement. One can wonder why digitation formation occurs for some BB
495 movements and not others. A possibility is that digitation formation depends both on
496 mechanical forces pulling the membrane and on cortical stiffness. BB movement and
497 digitation formation could thus depend on the balance between these two forces. It

498 would therefore be interesting to investigate the dynamics of cortical actin during BB
499 movements and digitation formation.

500 ***Possible role of microtubules in BB recruitment to Par3 patches***

501 Our results suggest that mechanical forces between Par3 and the BB could be
502 exerted by microtubules. Dynamic microtubules link the BB and Par3 patches before
503 BB movements and/or digitation formation. Microtubules are required for membrane
504 digitations formation in several systems ([32],[31]) and are thus very likely to transmit the
505 mechanical forces between BB and Par3 patches that lead to BB movements and/or
506 membrane digitations.

507 An interesting further question concerns the mechanisms that regulate microtubule
508 dynamics to lead to BB movements. BB movements towards Par3 patches could
509 involve local microtubule depolymerization at the patch (Fig. 8b), coupled to
510 microtubule anchoring by dynein as proposed for the migration of the centrosome
511 toward the immunological synapse ("end-on-capture-shrinkage" mechanism)([33]).
512 Indeed, Par3 can interact with Dynein ([34]) and also with microtubules, directly ([35]) or
513 indirectly via 14-3-3 proteins ([36]). Consistent with a role for cortical dynein, a recent
514 study in mouse ependymal multi-ciliated cells showed a role of cortical dynein in the
515 off-centering of BB clusters ([37]). Moreover, dynein cortical localization depends on
516 Daple, which is a known partner of Par3. Par3 could also regulate microtubule
517 depolymerization via Rac1, which mediates Par3 function in the mouse cochlea ([38]).
518 In different systems, Par3 regulates the local activity of Rac via the RacGEFs Tiam1
519 and Trio ([39],[40],[41]). Par3 can increase microtubule catastrophe rate by inhibiting Trio in
520 neural crest cells ([42]), and Rac1 can regulate microtubule dynamics via CLIP-170 or
521 Stathmin in other systems ([43],[44]).

522 Interestingly, microtubules also actively maintain BB polarity at later stages, as
523 recently demonstrated ([21]), but the authors could not distinguish between a role of
524 microtubules as mechanical forces generators or as tracks for PCP proteins transport
525 and asymmetric localization: indeed in nocodazole-treated embryos, Vangl2
526 asymmetric localization is lost. This is an important caveat for studies that will try to
527 address the role of microtubules in BB positioning in a PCP context in more details,
528 since microtubules role in PCP protein transport and asymmetric localization seems
529 to be widely conserved ([45],[46]). Finally, Par3 apical localization also depends on
530 microtubules in zebrafish embryo neural tube ([47]): thus it might prove difficult to
531 disentangle the different potential roles of microtubules in the asymmetric positioning
532 of BBs of planar polarized ciliated epithelia.

533 ***The core PCP protein Vangl2 is involved in BB positioning via Par3***
534 ***enrichment to the posterior membrane***

535 In *vangl2*$^{m209/m209}$ embryos, BBs show behavioral defects, making more lateral
536 movements and more contacts with lateral membranes than in wt embryos.
537 Strikingly, in *vangl2* mutants as in wt, BBs always contacted the apical junctions at
538 Par3-positive patches. The altered behavior of BBs in *vangl2*$^{m209/m209}$ embryos
539 correlated with a mislocalization of Par3 around the apical junctions of FP cells. Since
540 Par3 mislocalization affected BB polarization, we propose that Par3 posterior
541 enrichment and patch formation under the control of the PCP pathway is a main actor
542 in BB posterior positioning (Fig.8a).

543 How PCP proteins act on Par3 localization in the FP remains to be uncovered. In FP
544 cells, Vangl2 localizes anteriorly ([48]); thus, Vangl2 effect on Par3 could be mediated
545 by Dvl. Indeed, Vangl2 is required for proper asymmetric localization of Dvl in planar

546 polarized tissues and Dvl can recruit Par3 to the posterior membrane in Drosophila
547 sensory organ precursors ([49]). Dvl could also recruit Par3 via Daple, as this protein
548 colocalizes with Par3 in the mouse cochlea and can bind both Dvl and Par3 in yeast
549 two-hybrid assays ([50]). Recent studies have shown that Par3 is asymmetrically
550 localized within the plane of the epithelium in several systems, like Drosophila
551 ommatidia ([51]) and sensory organ precursors just before asymmetric division ([52]), in
552 Xenopus embryo ectoderm ([53]) and in the mouse cochlea ([38]), suggesting that in
553 addition to its classical role in apico-basal polarization, Par3 might also be involved in
554 PCP across species and even considered a bona fide core PCP protein. It will be
555 interesting to investigate whether this Par3 posterior enrichment involves a positive
556 feedback loop between BB and Par3 patches either directly by contact ([54]) or via
557 dynamic microtubule (+) ends ([55]).

558 Finally, as asymmetric centriole positioning is now recognized as a conserved
559 readout of PCP ([56],[57]), it will be interesting to investigate whether Par3 has a
560 conserved role in centriole/BB positioning in other species where BB/centriole off-
561 centering has been described and also depends on PCP proteins, for example in the
562 embryo of the jellyfish Clytia *hemisphaerica* ([58]) or in Drosophila pupal wing ([56]).

563

564

565

566 MATERIALS AND METHODS

567 Zebrafish handling and experimentation

568 Wild-type and mutant zebrafish embryos were obtained by natural spawning. We
569 used wild-type AB or (TL x AB) hybrid strains, *vangl2*^{m209} mutants ([30], ZDB-GENO-
570 190204-5), *par3ab fh305* mutants ([27], ZDB-FISH-150901-20689) and created a
571 transgenic Netrin-KalTA4 line, expressing the KalTA4 transcriptional activator in
572 floor-plate cells. The Netrin-KalTA4 line was generated by injecting at the 1 cell stage
573 15pg of pNetrin-KalTA4 plasmid along with 20pg of Tol2 mRNA. To obtain the early
574 stages (4-8s), embryos were collected at 10 am and incubated for 9 h in a 33°C
575 incubator. To obtain later stages (14-20s), embryos were collected at 10 am and
576 incubated for 2 h at 28 °C before being placed overnight in a 24 °C incubator. All our
577 experiments were made in agreement with the European Directive 210/63/EU on the
578 protection of animals used for scientific purposes, and the French application decree
579 'Décret 2013-118'. The projects of our group have been approved by our local ethical
580 committee 'Comité d'éthique Charles Darwin'. The authorization number is
581 2015051912122771 v7 (APAFIS#957). The fish facility has been approved by the
582 French 'Service for animal protection and health' with approval number A-75-05-25.

583

584 Plasmid construction

585 **pUAS:flag-aPKC**: the rat aPKC (PKC zeta) coding sequence was amplified by
586 PCR from addgene plasmid #10799 using primers (flagaPKC-forward and reverse)
587 with 15bp 5' and 3' overhangs. Primers homologous to these overhangs (UASRho-
588 forward and reverse) were used to amplify the backbone of the pUAS-RhoAwt
589 plasmid (Hanovice 2016) (thus removing the mCherry-RhoA sequence). The two

590 DNA fragments were then ligated into one plasmid with the InFusion HD cloning kit
591 (Takara).

592 **pNetrin:KalTA4**: a 1.4kb fragment from pCSKalTA4 comprising the KalTA4
593 promoter was amplified using the KalTA4-forward and KalTA4-reverse primers, then
594 digested with XhoI and NotI (NEB) and placed under the control of the floor-plate
595 specific 898bp Netrin1 enhancer ([59]) from a XhoI/NotI-digested
596 pNetrin898:membCherry plasmid (Marie Breau, unpublished) by ligation with the T4
597 DNA ligase (NEB).

598

599 **mRNA, morpholino and plasmids injection**

600 mRNAs were synthesized from linearized pCS2 vectors using the mMESSAGE
601 mMACHINE SP6 transcription kit (Ambion). The following amounts of mRNA were
602 injected into one-cell stage embryos: 22 pg for Centrin-GFP, 40 pg for mbCherry
603 (membrane Cherry) or Membrane-GFP (Gap43-GFP). For Par3-RFP mosaic
604 expression, mRNAs were injected at the 16-cell stage in a single blastomere, using
605 50 pg for Par3-RFP live-imaging or 150pg Par3-RFP for over-expression experiments
606 along with Centrin-GFP and membrane-GFP mRNAs at the same concentration as
607 for one-cell stage injections. Par3ab-MO was injected at a concentration of 0.3 mM at
608 one-cell stage. For triple MO injections (Par3aa, ab and ba coinjection) each MO was
609 diluted to 0.25 mM. MO sequences are given in the supplementary methods.

610 For flag-aPKC mosaic experiments, 25pg of pUAS:flag-aPKC were injected in
611 NetKalTA4 embryos at the 1 cell stage. This leads to mosaic expression due both to
612 the stochastic expression of KalTA4 and the mosaic delivery of plasmid to some cells

613 and not others.

614 Immunostaining

615 For immunostaining, embryos were fixed in Dent fixative (80% Methanol, 20%
616 DMSO) at 25°C for 2 h, blocked in 5% goat serum, 1% bovine serum albumin and
617 0.3% triton in PBS for 1 h at room temperature and incubated overnight at 4 °C with
618 primary antibodies and 2 h at room temperature with secondary antibodies. The yolk
619 was then removed and the embryo mounted dorsal side up in Vectashield medium on
620 a slide. Imaging was done using a Leica TCS SP5 AOBS upright confocal
621 microscope using a 63X oil lens. A list of antibodies is given in the supplementary
622 methods.

623 Live imaging

624 Embryos were dechorionated manually and mounted in 0.5% low-melting agarose in
625 E3 medium. Movies were recorded at the temperature of the imaging facility room (22
626 °C) on a Leica TCS SP5 AOBS upright confocal microscope using a 63X (NA 0.9)
627 water immersion lens. The embryos were mounted either with dorsal side up (for
628 early stages or after 18s, when FP cells apical surface is quite large) or on the side
629 (for most 13-18s embryos, when the apical surface of FP cells is narrower and when
630 the images are more blurred when taken from a dorsal view, maybe because of the
631 thickness of the overlying neural tube). The anterior side of the embryos was
632 positioned on the left and their antero-posterior axis aligned horizontally. A z-stack
633 was acquired every 2 or 5min (or in some rarer cases every 4min) for most analysis
634 (Δt2min and Δt5min movies) and every 10sec for some movies (digitations analysis
635 and microtubule dynamics in Fig.S2, Δt10sec) with a z-step of 0.3μm. For each time-

636 point the z-stack extended from the most dorsal side of the notochord to neural cells
637 above the FP for Δt2min and Δt5min movies but was narrower for Δt10sec movies (to
638 allow fast acquisition and reduce photobleaching and photodamage). For embryos
639 mounted on the side, the z-stack extended through all the width of the FP. In every
640 case, the z-stack encompassed FP cells apical surface with the moving BBs. For
641 each time-point we then make a z-projection from a 3μm thick substack that
642 encompass the apical centrioles/BB.

643

644 **In situ hybridization**

645 Embryos at the 16 s and 24 hpf were processed as previously described ([60]).
646 Matrices for probe synthesis were synthesized by PCR using either adult genomic
647 DNA (for *par3aa*, *ba* and *bb*) or cDNA from 18 s embryos (for *par3ab*). Primer
648 sequences are available in the supplementary methods.

649 **Quantification and statistical analysis**

650 All bar-plots, boxplot and violin plots and statistical tests (Wilcoxon or Fisher tests,
651 see figure legends) were generated with R (version 3.3.2) and Rstudio (Version
652 1.1.463). ns (non-significant): $p>0.05$, *: $p<0.05$, **: $p<0.01$, ***: $p<0.001$, ****:
653 $p<0.0001$.

654 **BB position and movements**

655 In all our images, the antero-posterior axis (easily visualized thanks to the underlying
656 notochord, whose cells have an elongated shape orthogonal to the antero-posterior
657 axis) is horizontal and the anterior side of the embryo is toward the left. To assess
658 the polarization of FP cells, we used FIJI to first make a z-projection of thickness 3μm

659 around the centrioles. We then manually measured the distance "a" by drawing a line
660 between the most posterior centriole and the posterior membrane that was parallel to
661 the antero-posterior axis of the embryo (ie parallel to the horizontal axis of the image)
662 and the distance "b" by drawing a similar line, at the same level and also parallel to
663 the antero-posterior axis, between the anterior and posterior membrane (Fig. 1a,
664 dorsal view). We used a similar method for embryos mounted on the side (Fig. 1a
665 lateral view). The polarization index (p.i.) was then calculated as 1-(a/b). In some rare
666 cases, the transverse membranes in our z-projection around the centrioles are blurry
667 (Fig.2b); in these cases however, going slightly more basally through the z-stack
668 allows us to see a sharper membrane which is usually located just beneath the
669 boundary of the above blurry region.

670 To follow the evolution of polarization index, the distances "a" and "b" were measured
671 manually at each time-frame in FIJI. These distances and the polarization index were
672 then plotted using python matplotlib (Python 2.7.13) and analyzed with a custom
673 python script to extract relevant information such as the frequency of contact with
674 posterior membrane or percentage of total time spent in contact with posterior
675 membrane. (Fig2 and FigS1).

676 For automatic tracking of BB movements (Fig5), BB were tracked using Image J
677 TrackMate ([61]). The movements were then manually curated to only keep active BB
678 movements and not BB movements due to global shift of cells (especially at early
679 stages when convergence-extension movements are still important), and to indicate
680 whether a contact with an anterior, posterior or lateral membrane occurred. The
681 results were then processed using a custom python script to calculate each
682 movement length and angle relative to the horizontal axis (ie the antero-posterior axis

683 of the embryo) and plotted using Python Matplotlib and R ggplot2. We defined
684 antero-posterior movements as the ones with angles relative to horizontal axis
685 inferior to 45° (ie in the intervals [315-45°[and [135-225°[in Fig. 6a).

686 For all analyzes, lateral membranes are defined as the ones more parallel to the
687 horizontal axis and transverse membranes as the ones more orthogonal to the
688 horizontal axis. The transition between lateral and transverse (anterior and posterior)
689 membranes is evidenced by "Y"-shaped tri-cellular junctions (as in Fig. 4a) or sharp
690 turns in the membrane (as in Fig. 7f).

691 **Par3-RFP posterior/anterior ratio**

692 Fluorescence intensity was measured along the anterior-posterior length of isolated
693 labelled FP cells in FIJI. A custom python script was then used to extract the first
694 quarter (cell anterior side) and last quarter (cell posterior side) of fluorescence
695 intensity values, to determine the area under each curve (corresponding to
696 fluorescence intensity), calculate the post/ant ratio and plot it along with the
697 polarization index (see BB movements analysis section).

698 **Par3 peaks quantification**

699 Fluorescence intensity from immunostained embryos was measured along FP cells
700 transverse membranes and exported to Matlab (R2018a). For each cell, the
701 "findpeaks" function was used to detect Par3 fluoresence peaks and measure their
702 prominence, which was then normalized by the minimal Par3 fluorescence value
703 along the junction.

704

705 **Additional softwares**

706 Adobe Photoshop was used to assemble the figures. Fig. 1a was done in Microsoft
707 Powerpoint and Fig. 8 with Adobe Illustrator.

708

709 ## ACKNOWLEDGEMENTS

710

711 We are grateful to the aquatic animal and cell imaging facilities of the IBPS (Institut
712 de Biologie Paris-Seine FR3631, Sorbonne Université, CNRS, Paris, France) for their
713 technical assistance. We thank Teresa Ferraro for sharing her expertise in image
714 analysis, Marie Breau for her help in setting up the live imaging protocol, Isabelle
715 Anselme for participation in genotyping and Sophie Gournet for her help in the design
716 of Fig. 8. We thank Paula Alexandre for the kind gift of Par3-RFP construct, Andreas
717 Wodarz for the BazP1085 antibody, Maximilien Furthauer for the *vangl2*^{m209} line. We
718 thank Nicolas David and Marie Breau for critical reading and insightful comments on
719 the manuscript. This work was supported by funding from the Agence Nationale pour
720 la Recherche (ANR, project CILIAINTHEBRAIN to SSM) and the Fondation pour la
721 Recherche Médicale (Equipe FRM DEQ20140329544 and EQU201903007943 funding
722 to SSM). A.D was supported by fellowships from the Ecole Normale Supérieure de
723 Cachan and from the Fondation ARC contre le Cancer. The authors declare no
724 competing financial interests.

725

726

727

728

729 **REFERENCES**

730

731 1. Wallingford, J. B. Planar cell polarity signaling, cilia and polarized ciliary beating.
732 *Current Opinion in Cell Biology* **22**, 597–604 (2010).
733 2. Meunier, A. & Azimzadeh, J. Multiciliated Cells in Animals. *Cold Spring Harb*
734 *Perspect Biol* **8**, a028233 (2016).
735 3. Montcouquiol, M. *et al.* Identification of Vangl2 and Scrb1 as planar polarity genes
736 in mammals. **423**, 5 (2003).
737 4. Mitchell, B. *et al.* The PCP Pathway Instructs the Planar Orientation of Ciliated
738 Cells in the Xenopus Larval Skin. *Current Biology* **19**, 924–929 (2009).
739 5. Borovina, A., Superina, S., Voskas, D. & Ciruna, B. Vangl2 directs the posterior
740 tilting and asymmetric localization of motile primary cilia. *Nature Cell Biology* **12**, 407–
741 412 (2010).
742 6. Mirzadeh, Z., Han, Y.-G., Soriano-Navarro, M., Garcia-Verdugo, J. M. & Alvarez-
743 Buylla, A. Cilia Organize Ependymal Planar Polarity. *Journal of Neuroscience* **30**, 2600–
744 2610 (2010).
745 7. Song, H. *et al.* Planar cell polarity breaks bilateral symmetry by controlling ciliary
746 positioning. *Nature* **466**, 378–382 (2010).
747 8. Boutin, C., Goffinet, A. M. & Tissir, F. Chapter Seven - Celsr1–3 Cadherins in PCP
748 and Brain Development. in *Current Topics in Developmental Biology* (ed. Yang, Y.) vol.
749 101 161–183 (Academic Press, 2012).
750 9. Hirota, Y. *et al.* Planar polarity of multiciliated ependymal cells involves the
751 anterior migration of basal bodies regulated by non-muscle myosin II. *Development* **137**,
752 3037–3046 (2010).
753 10. Hegan, P. S., Ostertag, E., Geurts, A. M. & Mooseker, M. S. Myosin Id is required for

754 planar cell polarity in ciliated tracheal and ependymal epithelial cells. *Cytoskeleton* **72**,
755 503–516 (2015).
756 11. Hashimoto, M. *et al.* Planar polarization of node cells determines the rotational
757 axis of node cilia. *Nature Cell Biology* **12**, 170–176 (2010).
758 12. Grimsley-Myers, C. M., Sipe, C. W., Geleoc, G. S. G. & Lu, X. The Small GTPase Rac1
759 Regulates Auditory Hair Cell Morphogenesis. *Journal of Neuroscience* **29**, 15859–15869
760 (2009).
761 13. Ezan, J. *et al.* Primary cilium migration depends on G-protein signalling control of
762 subapical cytoskeleton. *Nature Cell Biology* **15**, 1107–1115 (2013).
763 14. Tarchini, B., Jolicoeur, C. & Cayouette, M. A Molecular Blueprint at the Apical
764 Surface Establishes Planar Asymmetry in Cochlear Hair Cells. *Developmental Cell* **27**, 88–
765 102 (2013).
766 15. Ross, A. J. *et al.* Disruption of Bardet-Biedl syndrome ciliary proteins perturbs
767 planar cell polarity in vertebrates. *Nature Genetics* **37**, 1135–1140 (2005).
768 16. Jones, C. *et al.* Ciliary proteins link basal body polarization to planar cell polarity
769 regulation. *Nature Genetics* **40**, 69–77 (2008).
770 17. Mahuzier, A. *et al.* Dishevelled stabilization by the ciliopathy protein Rpgrip1l is
771 essential for planar cell polarity. *The Journal of Cell Biology* **198**, 927–940 (2012).
772 18. Ohata, S. *et al.* Mechanosensory Genes Pkd1 and Pkd2 Contribute to the Planar
773 Polarization of Brain Ventricular Epithelium. *Journal of Neuroscience* **35**, 11153–11168
774 (2015).
775 19. Lepelletier, L., de Monvel, J. B., Buisson, J., Desdouets, C. & Petit, C. Auditory Hair
776 Cell Centrioles Undergo Confined Brownian Motion Throughout the Developmental
777 Migration of the Kinocilium. *Biophysical Journal* **105**, 48–58 (2013).
778 20. Thouvenin, O. *et al.* Origin and role of the cerebrospinal fluid bidirectional flow in

779 the central canal. *eLife* **9**, e47699 (2020).

780 21. Mathewson, A. W., Berman, D. G. & Moens, C. B. Microtubules are required for the
781 maintenance of planar cell polarity in monociliated floorplate cells. *Developmental*
782 *Biology* (2019) doi:10.1016/j.ydbio.2019.04.007.

783 22. Fame, R. M., Chang, J. T., Hong, A., Aponte-Santiago, N. A. & Sive, H. Directional
784 cerebrospinal fluid movement between brain ventricles in larval zebrafish. *Fluids and*
785 *Barriers of the CNS* **13**, (2016).

786 23. Sepich, D. S., Usmani, M., Pawlicki, S. & Solnica-Krezel, L. Wnt/PCP signaling
787 controls intracellular position of MTOCs during gastrulation convergence and extension
788 movements. *Development* **138**, 543–552 (2011).

789 24. Inaba, M., Venkei, Z. G. & Yamashita, Y. M. The polarity protein Baz forms a
790 platform for the centrosome orientation during asymmetric stem cell division in the
791 Drosophila male germline. *Elife* **4**, e04960 (2015).

792 25. Jiang, T., McKinley, R. F. A., McGill, M. A., Angers, S. & Harris, T. J. C. A Par-1-Par-3-
793 Centrosome Cell Polarity Pathway and Its Tuning for Isotropic Cell Adhesion. *Current*
794 *Biology* **25**, 2701–2708 (2015).

795 26. Krahn, M. P., Egger-Adam, D. & Wodarz, A. PP2A Antagonizes Phosphorylation of
796 Bazooka by PAR-1 to Control Apical-Basal Polarity in Dividing Embryonic Neuroblasts.
797 *Developmental Cell* **16**, 901–908 (2009).

798 27. Blasky, A. J., Pan, L., Moens, C. B. & Appel, B. Pard3 regulates contact between
799 neural crest cells and the timing of Schwann cell differentiation but is not essential for
800 neural crest migration or myelination: PARD3 IN NC MIGRATION AND SCHWANN CELL
801 MYELINATION. *Developmental Dynamics* **243**, 1511–1523 (2014).

802 28. Liu, Z. *et al.* Par complex cluster formation mediated by phase separation. *Nat*
803 *Commun* **11**, 2266 (2020).

804 29. Distel, M., Wullimann, M. F. & Köster, R. W. Optimized Gal4 genetics for
805 permanent gene expression mapping in zebrafish. *Proceedings of the National Academy*
806 *of Sciences* **106**, 13365–13370 (2009).
807 30. Solnica-Krezel, L. *et al.* Mutations affecting cell fates and cellular rearrangements
808 during gastrulation in zebrafish. 14.
809 31. Redemann, S. *et al.* Membrane Invaginations Reveal Cortical Sites that Pull on
810 Mitotic Spindles in One-Cell C. elegans Embryos. *PLoS ONE* **5**, e12301 (2010).
811 32. Negishi, T., Miyazaki, N., Murata, K., Yasuo, H. & Ueno, N. Physical association
812 between a novel plasma-membrane structure and centrosome orients cell division. *eLife*
813 **5**, e16550 (2016).
814 33. Yi, J. *et al.* Centrosome repositioning in T cells is biphasic and driven by
815 microtubule end-on capture-shrinkage. *The Journal of Cell Biology* **202**, 779–792 (2013).
816 34. Schmoranzer, J. *et al.* Par3 and Dynein Associate to Regulate Local Microtubule
817 Dynamics and Centrosome Orientation during Migration. *Current Biology* **19**, 1065–
818 1074 (2009).
819 35. Chen, S. *et al.* Regulation of Microtubule Stability and Organization by Mammalian
820 Par3 in Specifying Neuronal Polarity. *Developmental Cell* **24**, 26–40 (2013).
821 36. Benton, R. & St Johnston, D. Drosophila PAR-1 and 14-3-3 inhibit Bazooka/PAR-3
822 to establish complementary cortical domains in polarized cells. *Cell* **115**, 691–704
823 (2003).
824 37. Takagishi, M., Esaki, N., Takahashi, K. & Takahashi, M. Cytoplasmic Dynein
825 Functions in Planar Polarization of Basal Bodies within Ciliated Cells. *iScience* **23**,
826 101213 (2020).
827 38. Landin Malt, A. *et al.* Par3 is essential for the establishment of planar cell polarity
828 of inner ear hair cells. *Proceedings of the National Academy of Sciences* 201816333

829 (2019) doi:10.1073/pnas.1816333116.

830 39. Nishimura, T. *et al.* PAR-6–PAR-3 mediates Cdc42-induced Rac activation through
831 the Rac GEFs STEF/Tiam1. *Nature Cell Biology* **7**, 270–277 (2005).

832 40. Matsuzawa, K. *et al.* PAR3-aPKC regulates Tiam1 by modulating suppressive
833 internal interactions. *Mol Biol Cell* **27**, 1511–1523 (2016).

834 41. Zhang, H. & Macara, I. G. The polarity protein PAR-3 and TIAM1 cooperate in
835 dendritic spine morphogenesis. *Nature Cell Biology* **8**, 227–237 (2006).

836 42. Moore, R. *et al.* Par3 controls neural crest migration by promoting microtubule
837 catastrophe during contact inhibition of locomotion. *Development* **140**, 4763–4775
838 (2013).

839 43. Fukata, M. *et al.* Rac1 and Cdc42 capture microtubules through IQGAP1 and CLIP-
840 170. *Cell* **109**, 873–885 (2002).

841 44. Wittmann, T., Bokoch, G. M. & Waterman-Storer, C. M. Regulation of Microtubule
842 Destabilizing Activity of Op18/Stathmin Downstream of Rac1. *Journal of Biological*
843 *Chemistry* **279**, 6196–6203 (2004).

844 45. Shimada, Y., Yonemura, S., Ohkura, H., Strutt, D. & Uemura, T. Polarized Transport
845 of Frizzled along the Planar Microtubule Arrays in Drosophila Wing Epithelium.
846 *Developmental Cell* **10**, 209–222 (2006).

847 46. Vladar, E. K., Bayly, R. D., Sangoram, A. M., Scott, M. P. & Axelrod, J. D.
848 Microtubules Enable the Planar Cell Polarity of Airway Cilia. *Current Biology* **22**, 2203–
849 2212 (2012).

850 47. Buckley, C. E. *et al.* Mirror-symmetric microtubule assembly and cell interactions
851 drive lumen formation in the zebrafish neural rod. *The EMBO Journal* **32**, 30–44 (2012).

852 48. Davey, C. F., Mathewson, A. W. & Moens, C. B. PCP Signaling between Migrating
853 Neurons and their Planar-Polarized Neuroepithelial Environment Controls Filopodial

854 Dynamics and Directional Migration. *PLOS Genetics* **12**, e1005934 (2016).
855 49. Banerjee, J. J. *et al.* Meru couples planar cell polarity with apical-basal polarity
856 during asymmetric cell division. *eLife* **6**, (2017).
857 50. Siletti, K., Tarchini, B. & Hudspeth, A. J. Daple coordinates organ-wide and cell-
858 intrinsic polarity to pattern inner-ear hair bundles. *Proceedings of the National Academy*
859 *of Sciences* 201716522 (2017) doi:10.1073/pnas.1716522115.
860 51. Aigouy, B. & Le Bivic, A. The PCP pathway regulates Baz planar distribution in
861 epithelial cells. *Scientific Reports* **6**, 33420 (2016).
862 52. Besson, C. *et al.* Planar Cell Polarity Breaks the Symmetry of PAR Protein
863 Distribution prior to Mitosis in Drosophila Sensory Organ Precursor Cells. *Current*
864 *Biology* **25**, 1104–1110 (2015).
865 53. Chuykin, I., Ossipova, O. & Sokol, S. Y. Par3 interacts with Prickle3 to generate
866 apical PCP complexes in the vertebrate neural plate. *eLife* **7**, e37881 (2018).
867 54. Saturno, D. M. *et al.* Sustained centrosome-cortical contact ensures robust
868 polarization of the one-cell C. elegans embryo. *Developmental Biology* (2017)
869 doi:10.1016/j.ydbio.2016.12.025.
870 55. Akhmanova, A., Stehbens, S. J. & Yap, A. S. Touch, Grasp, Deliver and Control:
871 Functional Cross-Talk Between Microtubules and Cell Adhesions. *Traffic* **10**, 268–274
872 (2009).
873 56. Carvajal-Gonzalez, J. M., Roman, A.-C. & Mlodzik, M. Positioning of centrioles is a
874 conserved readout of Frizzled planar cell polarity signalling. *Nature Communications* **7**,
875 11135 (2016).
876 57. Carvajal-Gonzalez, J. M., Mulero-Navarro, S. & Mlodzik, M. Centriole positioning in
877 epithelial cells and its intimate relationship with planar cell polarity. *BioEssays* **38**,
878 1234–1245 (2016).

879 58. Momose, T., Kraus, Y. & Houliston, E. A conserved function for Strabismus in
880 establishing planar cell polarity in the ciliated ectoderm during cnidarian larval
881 development. *Development* **139**, 4374–4382 (2012).
882 59. Rastegar, S. *et al.* A Floor Plate Enhancer of the Zebrafish netrin1 Gene Requires
883 Cyclops (Nodal) Signalling and the Winged Helix Transcription Factor FoxA2.
884 *Developmental Biology* **252**, 1–14 (2002).
885 60. Jowett, T. & Lettice, L. Whole-mount in situ hybridizationon zebrafish embryos
886 using a mixture of digoxigenin- and fluorescein-labelled probes. *Trends in Genetics* **10**,
887 73–74 (1994).
888 61. Tinevez, J.-Y. *et al.* TrackMate: An open and extensible platform for single-particle
889 tracking. *Methods* **115**, 80–90 (2017).
890 62. Wei, X. *et al.* The zebrafish Pard3 ortholog is required for separation of the eye
891 fields and retinal lamination. *Developmental Biology* **269**, 286–301 (2004).
892 63. Megason, S. G. In Toto Imaging of Embryogenesis with Confocal Time-Lapse
893 Microscopy. in *Zebrafish* (eds. Lieschke, G. J., Oates, A. C. & Kawakami, K.) vol. 546 317–
894 332 (Humana Press, 2009).
895 64. Pouthas, F. *et al.* In migrating cells, the Golgi complex and the position of the
896 centrosome depend on geometrical constraints of the substratum. *Journal of Cell Science*
897 **121**, 2406–2414 (2008).
898 65. Alexandre, P., Reugels, A. M., Barker, D., Blanc, E. & Clarke, J. D. W. Neurons derive
899 from the more apical daughter in asymmetric divisions in the zebrafish neural tube.
900 *Nature Neuroscience* **13**, 673–679 (2010).
901 66. Hanovice, N. J., McMains, E. & Gross, J. M. A GAL4-inducible transgenic tool kit for
902 the in vivo modulation of Rho GTPase activity in zebrafish: Modulating Rho GTPase
903 Activity in zebrafish. *Developmental Dynamics* **245**, 844–853 (2016).

904 FIGURE LEGENDS

905

906 **Figure 1 Zebrafish floor-plate progressive planar polarization during**
907 **somitogenesis.**

908 **a)** Experimental set-up used to study floor-plate planar polarization in fixed or live
909 embryos. Early stage embryo (4-12s stages) or late (after 18s) stage embryos, which
910 displayed floor-plate cells with large apical surfaces were usually imaged from the top
911 (dorsal view, upper part of the figure, see also b)), whereas embryos at intermediate
912 stages (with narrower apical surfaces) were imaged from the side (lateral view,
913 bottom half of the figure). A polarization index (defined as p.i.=1-(a/b) where "a" is the
914 distance between the BB and the posterior membrane and "b" the distance between
915 anterior and posterior membranes) was used to quantify BB position along the
916 antero-posterior axis.

917 **b-c)** Time-course of floor-plate polarization between the 6 s and 26 s stages **b)**
918 Dorsal views of the floor-plate of flat-mounted embryos showing immunostaining
919 against Centrin (green, BB), ZO1 (magenta, apical junctions) and Acetylated-Tubulin
920 (white, cilia) at 12 s (left) and 26 s (right). Note that cilia are already visible at 12 s
921 but are much longer at 26 s. The yellow arrow points at an anterior BB associated to
922 a cilium. *Scale bar:* 2 *µ*m **c)** Quantification of BB position measured from immuno-
923 stained samples as shown in a. BB position along the anterior-posterior axis was
924 quantified using the polarization index. Cells were then allocated to different
925 categories depending on their polarization index for each developmental stage (6 s:
926 7embryos, 108 cells ; 8 s: 14 embryos, 224 cells ; 10 s: 14 embryos, 354 cells ; 12 s:
927 5 embryos, 156 cells ; 14 s: 9 embryos, 208 cells ; 16 s,: 9 embryos, 220 cells ; 18 s:

928 5 embryos, 143 cells ; 26 s: 4 embryos, 119 cells). Statistical significance was
929 assessed using a Wilcoxon test.

930

931 **Figure 2 Floor-plate planar polarization involves a change in basal body**
932 **(BB) motile behavior.**

933 **a-d)** Live imaging of BB movements during the polarization process. Images were
934 taken every 5 minutes; a selection of images is presented here from two early stage
935 embryos (**a, b,** movies between the 6 s and 9 s stages; **d** yellow arrow in b points at
936 an anterior contact event) and two late stage embryos (**c, d,** movies between the 18
937 s and 21 s stages). The distances between BBs and posterior membranes were then
938 plotted (green curve) along with the distance between the anterior and posterior
939 membranes (magenta curve) and the p.i. (dashed blue curve). Black arrows on the
940 graphs indicate the position of the images displayed on the left. **e)** Quantification of
941 the percentage of total movie time spent by the BB in contact with the posterior
942 membrane. (4-8s: 5 embryos, 41 cells; 13-17s: 6 embryos, 38 cells; 17-21s: 7
943 embryos, 59 cells). **f, g)** Number of contact events per h between BB and anterior (**f**)
944 or posterior (**g**) membrane in embryos filmed at different developmental stages: 4 to
945 8 s (5 embryos, 41 cells), 13 to 17 s (5 embryos, 25 cells) and 17 to 21 s (7 embryos,
946 32 cells). Cells with a BB in contact with the posterior membrane during the whole
947 movie (points at 100% in Fig. 1e) were not plotted in f and g. Statistical significance
948 was assessed using a Wilcoxon test. *Scale bars:* 2 μm.

949

950 **Figure 3 Membrane digitations link BBs to transverse membranes during**
951 **FP polarization**

952 **a)** Images taken from live-imaging (Δt = 2 or 5 min between two images) showing a
953 posterior digitation (top) and an anterior digitation (bottom) (white arrows). Time (in
954 min) is indicated in the upper-left corner. Short mbCherry-positive digitations,
955 presumably corresponding to cilia, were in some cases associated to the BB (yellow
956 arrowheads). These membrane digitations were rare in late stage embryos (6/57
957 cells out of 10 embryos) compared to early embryos (44/68 cells from 9 embryos),
958 suggesting that Mb-Cherry entry into cilia is less common at later stages, which could
959 reflect a maturation of the "ciliary gate", a set of proteins regulating entry in and exit
960 out of cilia. **b)** Proportion of posterior and anterior digitations (54 digitations, 8
961 embryos, 22 cells) **c)** Number of timepoints where anterior or posterior digitations
962 were detected in time-lapse movies with Δt = 2 or 5 minutes (Δt2min: 6 anterior, 23
963 posterior digitations, 4 embryos, 8 cells. Δt5min: 3 anterior and 22 posterior
964 digitations, 3 embryos, 13 cells, Wilcoxon tests) **d)** BB movements after anterior (left
965 bar) or posterior digitation (48 digitations, 8 embryos, 22 cells, Fisher test)

966

967

968

969 **Figure 4. Par3 is asymmetrically localized in FP cells and forms**
970 **patches at which almost all BB/membrane contacts occur.**

971 **a)** Individual cells from dorsal views of 14 s stage embryos showing IF with a Par3
972 antibody in FP cells. Two distinct cells are shown. Par3 localizes at apical junctions

973 and is enriched at tricellular junctions (yellow arrowhead) and in patches at
974 transverse membranes (white arrows), whether the BB is in contact with the posterior
975 membrane (left images) or not (right image). **b)** Representative images of mosaically
976 labelled FP cells expressing Par3-RFP and Centrin-GFP at early (8 s, left) or late (17
977 s, right) stages. Yellow arrows point at posterior Par3-RFP enrichment. Boxplots on
978 the right show quantification of Par3-RFP posterior/anterior fluorescence intensity
979 ratio in fully polarized FP cells at early and late stages. The red dotted line indicates a
980 ratio of 1 (corresponding to a symmetric Par3-RFP distribution) (6-12s, mean ratio=
981 1.42, 7 embryos, 9 cells; 14-20s mean ratio =1.38, 13 embryos, 21 cells, Wilcoxon
982 test). **c-d)** Images of time-lapse movies showing individual FP cells from embryos
983 mosaically expressing Par3-RFP (magenta) and centrin-GFP (green) (lateral view).
984 Par3-RFP posterior/anterior fluorescence intensity ratio is plotted on the right plots
985 (magenta curve) along with the polarization index (« p.i. », dashed blue curve). Black
986 arrows on plots indicate the time-points corresponding to the images displayed on the
987 left. **c)** FP cell with Par3 posterior enrichment in an embryo filmed between the 15 s
988 and 17 s stages. Par3 posterior enrichment starts 20 min after the beginning of the
989 movie (magenta arrow), 10 min before BB/posterior membrane contact (green
990 arrow). **d)** FP cell with no posterior Par3 enrichment (Par3-RFP post/ant ratio close
991 to 1) with a BB oscillating around the middle of the apical surface, in an embryo
992 filmed between 17 s and 19 s.
993 **e-f)** Images from time lapse movies of early stage embryos mosaically injected with
994 centrin-GFP (green), Membrane-GFP (green) and Par3-RFP (magenta) mRNAs. All
995 pictures are dorsal views of FP cells. **e)** global view of 6 adjacent FP cells; white
996 arrows point at Par3 patches (aligned along the AP axis) with which BB will make

997 contacts during the movie. **f)** Example of a BB moving back and forth and contacting
998 the membrane at Par3 patches. Posterior and anterior membrane digitations
999 originating from Par3 patches and partially coated with Par3 can also be seen. Yellow
1000 arrows point to posterior (t=0') and anterior (t=64') digitations. White arrowheads
1001 point to Par3 patches. Par3 patch deformation can be seen at t=64' and at t=0'
1002 (images on the right show a close-up on the framed region at t=0'). Scale bars: 2μm.
1003

1004 **Figure 5 Disruption of FP polarization by Par3 or aPKC overexpression**

1005 **a)** Polarization index (p.i., cf Fig. 1) of Par3-RFP negative and positive FP cells from
1006 embryos mosaically over-expressing Par3-RFP. Representative immunostaining
1007 pictures of FP from embryos mosaically over-expressing Par3-RFP are displayed on
1008 the left; yellow arrows point at mispositioned BBs in Par3-RFP over-expressing cells.
1009 (538 Par3RFP negative cells and 375 Par3RFP positive cells from 20 embryos)
1010 **b)** Polarization index of flag-aPKC negative and positive FP cells in Netrin-KalTA4
1011 embryos injected with a UAS:flag-aPKC construct (241 negative cells and 79 positive
1012 cells from 24 embryos). Representative immunostaining pictures of FP from embryos
1013 mosaically over-expressing flag-aPKC are displayed on the left; yellow arrows point
1014 at mispositioned BBs in flag-aPKC over-expressing cells.
1015 **c)** Par3 patches prominence is defined as the height of Par3 fluorescence peak
1016 relative to the highest and nearest valley (local fluorescence minimum). For each cell,
1017 prominence is normalized by the lowest Par3 intensity value. Right scheme: yellow
1018 arrows: tricellular junctions; white bar: orientation of the fluorescence measurement
1019 along the transverse membrane, star: position of Par3 patch

1020 **d)** Quantification of FP cell polarization index (upper plots) and Par3 patches
1021 prominence (bottom plots) in embryos mosaically expressing flag-aPKC. (experiment
1022 1: 9 embryos, 23 flag-aPKC positive and 70 negative cells. experiment 2: 6 embryos,
1023 20 flag-aPKC positive and 56 negative cells).
1024 Scale bar: 2μm. Comparison was done using a Wilcoxon test.
1025

1026 **Figure 6 Abnormal BB behaviors in *vangl2*^{m209} mutant FP**

1027 **a)** BB movements in wt (left column) and *vangl2*^{m209} (right column) embryos at early
1028 (first line) and late (second line) developmental stages. Each dot represents the
1029 endpoint of a single BB movement, the starting point being the center of the circle;
1030 thus, the angles outside the circle represent BB movements orientation relative to the
1031 embryo anteroposterior axis, and the distance relative to the center of the circle
1032 represents its length (each circle radius corresponds to 7 μm). The color of the dots
1033 indicates whether a movements leads to a membrane contact and, if so, the nature of
1034 the contact (anterior, posterior or lateral). (early stages: wt 8 embryos, 20 cells, 238
1035 movements; *vangl2*^{m209}: 9 embryos, 20 cells, 220 movements. Late stages: wt 4
1036 embryos, 19 cells, 255 movements; *vangl2*^{m209}: 4 embryos, 42 cells, 708
1037 movements).

1038 **b, c)** Orientation of BB movements in wt and *vangl2*^{m209} embryos at early (b) or late
1039 (c) stages. **d, e)** BB movements speed , nature of membrane contacts and total time
1040 spent in contact with membranes at early (d) and late (e) stages.

1041 Statistical tests: Wilcoxon test for comparison of BB speeds; Fisher test for
1042 comparison of BB movements orientation and BB/membrane contacts.

1043 **Figure 7 Par3 clustering and localization in *vangl2*^{m209} mutant FP**

1044 **a)** Polarization index of *vangl2*$^{m209/m209}$ determined from immunostaining data wt: 2
1045 embryos, 49 cells; *vangl2*$^{m209/+}$: 3 embryos, 66 cells; *vangl2*$^{m209/m209}$: 5 embryos, 57
1046 cells. **b)** Immunostaining of phoshorylated Par3 (BazP1085 antibody) in *vangl2*$^{+/+}$
1047 (wt) and *vangl2*$^{m209/m209}$ embryo FP at 18 s. In each case ZO1 staining was removed
1048 in the right image to reveal Par3 patches (yellow arrows). **c)** Quantification of the
1049 number of Par3 patches per cell on transverse membranes from immunostaining
1050 data as shown in b. d) Prominence of Par3 patches (BazP1085 antibody) in wt and
1051 *vangl2*$^{m209/m209}$ mutant embryo FP at 18 s In a-d, *vangl2*$^{+/+}$: 7 embryos, 186 cells ;
1052 *vangl2*$^{m209/+}$: 5 embryos, 112 cells ; *vangl2*$^{m209/m209}$: 7 embryos, 129 cells. **e)**
1053 Percentage of cells displaying a lateral Par3-RFP patch in live-imaging experiments
1054 (such as the one described in f). *vangl2*$^{+/+}$ and *vangl2*$^{m209/+}$: 16 embryos, 45 cells ;
1055 *vangl2*$^{m209/m209}$: 7 embryos, 17 cells. **f)** Images from movies of 5s
1056 *vangl2*$^{m209/m209}$ embryos mosaically injected with Par3-RFP, Centrin-GFP and
1057 Membrane-GFP mRNA at the 16-32 cell stage. Yellow arrows point at contact events
1058 between lateral Par3 patches and BBs.

1059 Statistical tests: Wilcoxon test for comparison of p.i. and prominence; Fisher test for
1060 comparison of patch number and percentage of cells with lateral patches.

1061 **Figure 8 Summary of the main findings and hypothetical mechanism**

1062 **a)** Scheme showing BB behavior at early and late stages in the FP of wt and vangl2
1063 mutants. In wt at early stages of polarization, the BB makes back and forth
1064 movements (dotted lines) between anterior and posterior Par3 patches (magenta) but
1065 very few lateral movements. In contrast, in *vangl2* mutants, BBs make more lateral

1066 movements and contacts and these contacts always occur at ectopic lateral Par3
1067 patches. At later stages, the BB displays low motility. In wt, BBs are either docked to
1068 posterior Par3 patch or move in the posterior side of the cell, close to the patch,
1069 whereas in *vangl2* mutants BBs move around the center of the apical surface, which
1070 is probably due to earlier polarization defects and the still abnormal dispersion of
1071 Par3 patches around the apical junctions. Note that in both wt and *vangl2* embryos,
1072 at all stages studied, cilia are present and do not seem to impair BB movements.

1073 **b)** Hypothetical microtubule-based mechanism for BB polarization.

1074 Within the apical surface, dynamic microtubules emanate in all direction from the BB
1075 but can be captured at Par3 patches, at which their depolymerization is triggered (in
1076 this case at the posterior patch). The resulting mechanical force pulls on the
1077 membrane and the BB, which can result in digitation formation and/or BB movement
1078 towards the patch. The posterior Par3 enrichment makes it more likely for posterior
1079 pulling to happen (compared to anterior pulling) which ultimately results in a stably
1080 docked posterior BB at later stages.

1081

1082

1083 # SUPPLEMENTARY INFORMATION

1084 ## Methods

1085 ### Antibodies

Antibody	Source	Identifier	Dilution
Mouse monoclonal IgG2a anti-centrin (clone 20H5)	Merck Millipore	# 04-1624 RRID: AB_10563501	1:200
Mouse monoclonal IgG1 anti-ZO1 (clone ZO1-1A12)	Invitrogen	RRID: AB_2533147	1:400
Mouse monoclonal IgG2b anti-acetylated-tubulin (clone 6-11B-1)	Sigma-Aldrich	#T 6793 RRID: AB_477585	1:400
Rabbit polyclonal anti-Par3	Merck Millipore	#07-330 RRID:AB_11213581	1:200
Rabbit polyclonal anti-phosphorylated-Ser1085-Bazooka	[26]	N/A	1:200
Rabbit polyclonal anti-DsRed	Takara	# 632496 RRID:AB_10013483	1:400
Mouse IgG1 anti-FLAG (M2)	Sigma	F3165	1:100
Goat anti-mouse IgG1 Alexa633	Molecular probes	# A-21126 RRID:AB_2535768	1:400

Goat anti-mouse IgG2a Alexa568	Molecular probes	# A-21134 RRID:AB_2535773	1:400
Goat anti-mouse IgG2a Alexa488	Molecular probes	# A-21131 RRID:AB_141618	1:400
Goat anti-mouse IgG2b Alexa633	Molecular probes	# A-21146 RRID:AB_2535782	1:400
Goat anti-rabbit IgG Alexa568	Molecular probes	# A-11011 RRID:AB_143157	1:400

1086

1087 ## Oligonucleotides, Plasmides and Morpholinos

1088

Construct/oligonucleotide	Source
Par3ab-MO tcaaaggctcccgtgctctggtgtc	[62]
Par3aa-MO attcgcccgatattcccggagactc	this paper
Par3ba-MO ccgaaaatgaccgtcaccttcatct	this paper
Par3aa-forward gacaaccccgtaaaaaccccag	this paper
Par3aa-reverse taatacgactcactatagg tccccaccataatctctaagccc	this paper
Par3ab-forward ggctgatgagattaacctcacacaatg	this paper

Par3ab-reverse taatacgactcactataggcctgctcgcttatttttcccctg	this paper
Par3ba-forward gcctgttgacgaatatccaaaccag	this paper
Par3ba-reverse taatacgactcactataggcaacggttacaggttttcacctttct	this paper
Par3bb-forward gcaccagctgaccctaatgagt	this paper
Par3bb-reverse taatacgactcactatagg cactcatgaagtgaatcatgctgtcg	this paper
KalTA4-forward atgcctcgaggccaccatg	this paper
KalTA4-reverse cggttacgtaacccgggccat	this paper
flagaPKC-forward aaagcaggctttgcc aaa catggactataaggacgatgatgac	this paper
flagaPKC-reverse caagaaagctgggtc atcgatacgcgtggtaccaga	this paper
UASRho-forward gacccagctttcttgtacaaagtgg	this paper
UASRho-reverse ggcaaagcctgctttttgtac	this paper

pCS2-Membrane-Cherry	[63]
pCS2-GFPhumcentrin1	[64]
pCS2+-Par3-RFP	[65]
pCS-Gap43-GFP	David Wilkinson, unpublished
pUAS:mCherry-F2A-myc-RhoA^{W1}	[66]
pFLAG.PKCzeta	Addgene #10799
pUAS-flag-aPKC	this paper
pCSKalTA4	[29]
pNetrin898:membCherry	Marie Breau, unpublished
pNetrinKalTA4	this paper

1089

1090

1091

1092

1093

1094

1095

1096

1097

1098

1099

1100 SUPPLEMENTARY FIGURE LEGENDS

1101 **Supplementary Figure S1: Further characterization of FP polarization in**
1102 **space and time.**

1103 **a)** Quantification of FP polarization along the AP axis at 12 s. Analysis was
1104 performed on fixed immunostained embryos as described in Fig. 1a. Comparison
1105 between stages was done using a Wilcoxon test.

1106 **b)** Still images from FP BB (green) and membrane (magenta) live imaging (dorsal
1107 view, start at 14s stage). The yellow arrow points to BB that will move and make
1108 contacts with the posterior membrane between 0 and 50 min after the movie started.
1109 White arrowheads point at BBs in adjacent cells that stay in contact with the posterior
1110 membrane during this time interval. **c)** BB speed measured from live-imaging data at
1111 different developmental stages. The speed of each BB movement was calculated by
1112 dividing the value of BB/posterior membrane variations (corresponding to green
1113 curves in Fig. 1c-f) by the total duration of the movement (4-8s: 4 embryos, 38 cells;
1114 13-17s: 6 embryos, 22 cells; 17-21s: 7 embryos, 32 cells). Comparison between
1115 stages was done using a Wilcoxon test. **d)** Movies described in Fig. 1 were used to
1116 quantify BB direction change frequency, mean duration of BB/posterior membrane
1117 contact events as a percentage of total imaging duration and mean polarization index
1118 during live-imaging. Plots in the first line take into account the BBs that stay in
1119 contact with the posterior membrane 100% of movie duration (posteriorly docked
1120 BBs) whereas the second line only represents BBs that are not posteriorly docked.
1121 Comparison between stages was done using a Wilcoxon test. Scale bar: 2μm.

1122

1123 **Supplementary Figure S2: High temporal resolution imaging reveals**
1124 **numerous anterior and posterior digitations and dynamic microtubules**
1125 **between BB and target membrane**

1126 a-c) Characterization of digitations with high temporal resolution live-imaging (one
1127 image every 10sec) (12 embryos, 20 cells, 44 anterior digitations, 44 posterior
1128 digitations, 7 lateral digitations). **a)** Repartition of digitation types. Anterior, lateral and
1129 posterior correspond to the membrane from which the digitation forms. There were as
1130 many anterior as posterior digitations, in contrast to what we observe in our Δt=2 or 5
1131 min movies (Fig. 3) **b)** Quantification of digitation lifetime, recurrence time (time
1132 elapsed before a particular digitation reforms at the same spot) and maximal length.
1133 Dots in magenta correspond to digitations that had formed before the beginning of
1134 live-imaging or had not disappeared yet when we stopped filming, and for which we
1135 could not determine the exact lifetime (which is thus under-estimated) (comparison
1136 done with Wilcoxon test). **c)** Direction of BB movements after an anterior (left) or
1137 posterior (right) digitation disappears. The BB either moved anteriorly, posteriorly or
1138 remained still (comparison done with Fisher test).

1139 There was no difference in digitation lifetime, which median value was 50sec both for
1140 anterior and posterior digitations. The time elapsed between two recurrent digitations
1141 was also not significantly different between anterior (median of 70sec) and posterior
1142 (median of 80sec) digitations. The presence of more posterior digitations in Δt2min
1143 and Δt5min movies but not in Δt10sec movies could be due to the fact that we miss
1144 most very short-lived digitations in Δt2min or Δt5min movies and that the short
1145 duration of our Δt10sec movies (in average 20min long) prevented us to see some
1146 long-lived digitations from extension to retraction (pink dots). Anterior and posterior

1147 digitations had similar size of around 2μm, although anterior digitations were slightly
1148 longer (2.4μm), probably due to the fact that BBs even at these early stages have a
1149 posteriorly biased position (Fig. S1d Mean polarization index plots). Posterior
1150 digitations were followed by a posteriorward BB movement in 40% of cases (16/40)
1151 whereas anterior digitations were followed by an anteriorward BB movement in only
1152 30% of cases (13/34) suggesting that digitation formation is probably not a cause but
1153 rather a consequence of BB movements.
1154 **d)** Dorsal view of a FP cell of a 5s stage embryo mosaically injected with Centrin-
1155 GFP (BB), EB3-GFP (microtubule plus ends) and Membrane-Cherry**,** which was then
1156 imaged every 10s. The dotted frame corresponds to the enlarged region on the right.
1157 Yellow arrows (10"): microtubule extending from the BB toward the spot of the
1158 posterior membrane that the BB will reach at t=90". White arrows: membrane
1159 digitation forming from the spot targeted by the microtubule highlighted at t=10" and
1160 toward the BB. **e)** Time elapsed between an EB3 comet reaching a membrane (such
1161 as in a at t=10") and the moment when a digitation forms or the BB starts moving
1162 towards this membrane (6 embryos, 10 cells, 58 EB3 comets).

1163

1164 **Supplementary Figure S3: Par3 phosphorylation in FP cells and rapid**
1165 **migration of centrosome to Par3 patches after mitosis**

1166 **a)** Individual cells from dorsal views of 14 s stage embryos showing IF with an
1167 antibody against Drosophila Par3 (Bazooka/Baz) phosphorylated on Ser1085
1168 (BazP1085) in FP cells. Two distinct cells are shown. phospho-Par3 displays the
1169 same patchy localization as total Par3 (Fig4a) White arrows point at patches at

1170 transverse membranes, which are present whether the BB is in contact with the
1171 posterior membrane (left images) or not (right image).

1172 **b)** Example of FP cell mitosis in an early stage (5s) embryo mosaically injected with
1173 Par3-RFP, Centrin-GFP and Membrane-GFP mRNAs and imaged every 4 minutes
1174 (MovieS12). Yellow arrows point at Par3-RFP patches, at the onset of mitosis (t=0')
1175 and after cytokinesis, when the centrosome makes contact with the Par3 patch, in the
1176 posterior daughter cell (t=32') and anterior daughter cell (t=36').

1177

1178

1179 **Supplementary Figure S4: *Par3ab* morphants or mutants have normal**
1180 **FP polarization and Par3 patches**

1181 **a)** FP polarization index (p.i.) in non-injected (NI) and Par3ab morpholino (MO)-
1182 injected embryos at 18s stage (NI : 9 embryos, 171 cells ; Par3ab MO : 16 embryos,
1183 244 cells). **b)** BazP1085 patch prominence (left) and number (right) in NI and Par3ab
1184 MO injected embryos at 18s stage. NI : 4, embryos, 66 cells ; Par3MO : 3 embryos,
1185 38. cells **c)** p.i. of maternal zygotic heterozygous (*MZpar3ab*$^{+/-}$) or homozygous
1186 (*Mpar3ab*$^{-/-}$) *par3ab* mutants at 18s stage. *MZpar3ab*$^{+/-}$: 7 embryos, 106 cells ;
1187 *MZpar3ab*$^{-/-}$: 9 embryos, 152 cells. **d)** Par3 patches prominence (left) and number
1188 (right) in maternal zygotic heterozygous (*MZpar3ab*$^{+/-}$) or homozygous (*MZpar3ab*$^{-/-}$)
1189 Par3ab mutants at 18s stage (*MZpar3ab*$^{+/-}$: 3 embryos, 27 cells ; *MZpar3ab*$^{-/-}$: 3
1190 embryos, 59 cells). p.i. and patch prominence are compared with a Wilcoxon test;
1191 Par3 or BazP1085 patches number are compared with Fisher test. **e)**
1192 Immunostaining of FP cells not injected (NI) or injected with Par3ab morpholino

1193 (Par3ab MO) showing the equivalent amount of BazP1085 staining in both
1194 conditions. **f)** Immunostaining of FP cells in *MZpar3ab*$^{+/-}$ and *MZpar3ab*$^{-/-}$ showing
1195 the equivalent amount of Par3 in both genotypes.

1196

1197 **Supplementary Figure S5: *par3aa/ab/ba* are broadly expressed during**
1198 **somitogenesis but their MO-mediated knockdown does not affect FP**
1199 **polarization**

1200 **a)** In situ hybridization reveals broad expression of *par3aa*, *ab* and *ba* genes at 16 s
1201 stage and 24 hpf. *par3bb* is not expressed at 16 s but is broadly expressed at 24 hpf
1202 with a posterior to anterior decreasing gradient. Scale bar 200*µ*m.

1203 **b)** Polarization index of 18 s stage embryos FP after coinjection of 3 MOs targeting
1204 *par3aa*, *ab* and *ba* at the one cell stage (non-injected: 4 embryos, 264 cells;
1205 morphants: 4 embryos, 133 cells).

1206 **c)** Global phosphorylated-Par3 immunostaining signal (sum of Par3 fluorescence on
1207 a similar portion of the floor-plate, a.u. arbitrary unit, 4 embryos for each condition).

1208 **d)** Phospho-Par3 patches prominence in non-injected embryos and triple morphants

1209 **e)** Number of phospho-Par3 patches per cell in non-injected embryos and triple
1210 morphants

1211 **f)** Immunostaining of FP cells in non-injected and triple morphants showing the
1212 presence of phospho-Par3 patches (white arrows) in both conditions.

1213 c-e) non-injected: 3 embryos, 76 cells; morphants 4 embryos, 83 cells. Scale bar:
1214 2*µ*m

1215 b,c,d) Comparison done with a Wilcoxon test, e) Comparison done with a Fisher test

1216

1217 SUPPLEMENTARY MOVIES LEGENDS

1218

1219 MovieS1: **Live imaging of a BB bouncing off the posterior membrane in**
1220 **an early-stage FP cell**.

1221 wt embryos were injected with Centrin-GFP (green) and membrane-Cherry
1222 (magenta) mRNAs at the one-cell stage. White arrows indicate the position of the BB
1223 at the first and last time-points. Images were taken every 5 minutes during the 6 s to
1224 9 s stages time-frame. Dorsal view. Corresponds to Fig2a.

1225

1226

1227 MovieS2: **Live imaging of a BB bouncing off posterior and anterior**
1228 **membranes in an early-stage FP cell**.

1229 wt embryos were injected with Centrin-GFP (green) and membrane-Cherry
1230 (magenta) mRNAs at the one-cell stage. White arrows indicate the position of the BB
1231 at the first and last time-points. Images were taken every 5 minutes during the 6 s to
1232 9 s stages time-frame. Dorsal view. Corresponds to Fig2b.

1233

1234 MovieS3: **Live imaging of a BB staying in contact with the posterior**
1235 **membrane in a late-stage FP cell**.

1236 wt embryos were injected with Centrin-GFP (green) and membrane-Cherry
1237 (magenta) mRNAs at the one-cell stage. White arrows indicate the position of the BB
1238 at the first and last time-points. Images were taken every 5 minutes during the 18 s to
1239 21 s stages time-frame. Dorsal view. Corresponds to Fig2c.

1240

1241

1242

1243 MovieS4: **Live imaging of BB bouncing against the posterior membrane in**

1244 **a late-stage FP cell**.

1245 wt embryos were injected with Centrin-GFP (green) and membrane-Cherry

1246 (magenta) mRNAs at the one-cell stage White arrows indicate the position of the BB

1247 at the first and last time-points. Images were taken every 5 minutes during the 18 s to

1248 21 s stages time-frame. Dorsal view. Corresponds to Fig2d.

1249

1250

1251 MovieS5: **Live imaging of BB movements in a FP cell displaying a**

1252 **membrane digitation between BB and the posterior membrane** (yellow

1253 arrow at t=115 min).

1254 wt embryos were injected with Centrin-GFP (green) and membrane-Cherry

1255 (magenta) mRNAs at the one-cell stage. White arrows point at the BB. Images were

1256 taken every 5 minutes during the 6 s to 9 s stages time-frame. Dorsal view.

1257 Corresponds to Fig3a upper row.

1258

1259 MovieS6: **Live imaging of BB movements in a FP cell displaying a**

1260 **membrane digitation between BB and the anterior membrane** (yellow

1261 arrow at t=18 min).

1262 wt embryos were injected with Centrin-GFP (green) and membrane-Cherry

1263 (magenta) mRNAs at the one-cell stage. Membrane digitations between the posterior

1264 membrane and BB can also be seen at t=10min, t=26min and t=66min. White arrows

1265 point at the BB. Images were taken every 2 minutes during the 8 s to 10 s stages
1266 time-frame. Dorsal view. Corresponds to Fig3a lower row.
1267
1268 MovieS7: **Live imaging of microtubule dynamics and BB movements in a**
1269 **FP cell at the 5s stage**.
1270 wt embryos were injected with EB3-GFP, Centrin-GFP (Fire LUT, coding for
1271 fluorescence intensity) and membrane-Cherry (green) mRNAs at the 16-cell stage.
1272 and then imaged for 8min every 10 seconds at the 5s stage. White arrow at t=0"
1273 points at the BB. White arrows at t=150", t=160", t=280" and t=290" point at posterior
1274 membrane deformation and yellow arrowheads at t=150" and t=280" point at
1275 microtubules linking BB and posterior membrane at the spot where the membrane
1276 bends and toward which BB will move. Dorsal view. Corresponds to FigS2d.
1277
1278 MovieS8: **Live imaging of BB movements and Par3-RFP localization in a**
1279 **polarizing FP cell**.
1280 wt embryos mosaically expressing Centrin-GFP (green) and Par3-RFP (magenta).
1281 White arrows point at the BB at t=0 and at t=30 min, when the BB touches the
1282 posterior membrane. Images were taken every 2 min during the 15 s to 17 s stages
1283 time-frame. Lateral view. Corresponds to Fig4c.
1284
1285
1286 MovieS9: **Live imaging of BB movements and Par3-RFP localization in a**
1287 **non-polarizing FP cell**.

1288 wt embryos mosaically expressing Centrin-GFP (green) and Par3-RFP (magenta).
1289 White arrows point at the BB at the beginning and end of movie. Images were taken
1290 every 5 minutes during the 17 s to 19 s stages time-frame. Lateral view. Corresponds
1291 to Fig4d.
1292
1293 MovieS10: **Live imaging of BB/Par3 patch contacts in an early-stage FP**
1294 **cell**.
1295 wt embryo mosaically expressing Centrin-GFP, Membrane-GFP (green) and Par3-
1296 RFP (magenta). White arrows point at the BB at the beginning of the movie, when the
1297 BB is in contact with the anterior Par3 patch, at t=30 min when it makes a contact
1298 with the posterior Par3 patch and at the end of the movie. Images were taken every 2
1299 min during the 4 s to 5 s stages time-frame. Dorsal view. Corresponds to the most
1300 anterior cell in Fig4e.
1301
1302 MovieS11: **Live imaging of membrane digitations at Par3 patches in early**
1303 **stage FP cells**.
1304 wt embryo mosaically expressing Centrin-GFP, Membrane-GFP (green) and Par3-
1305 RFP (magenta). White arrows point at the BB at the beginning and at the end of the
1306 movie. Yellow arrows at t=0 and t=68 min point at membrane digitations originating
1307 from the posterior and the anterior Par3 patches, respectively. Images were taken
1308 every 4 min during the 7 s to 8 s stages time-frame. Dorsal view. Corresponds to
1309 Fig4f.
1310

1311 MovieS12: **Live imaging of BB moving to Par3 patches after cytokinesis**
1312 **in dividing early stage FP cells**.
1313 wt embryo mosaically expressing Centrin-GFP, Membrane-GFP (green) and Par3-
1314 RFP (Fire LUT, coding for fluorescence intensity). Yellow arrows at t=0 point at the
1315 posterior and the anterior Par3 patches which are present in FP cells in interphase.
1316 Yellow arrows at t=32min and t=36min point at BB/Par3 patch contact in posterior
1317 and anterior daughter cells respectively. Images were taken every 4 min during the
1318 5s to 6s stages. Dorsal view. Corresponds to FigS3b.
1319
1320
1321 MovieS13: **Live imaging of BB/lateral Par3 patch contacts in an early-**
1322 **stage FP cell of a *vangl2*$^{m209/m209}$ mutant**.
1323 *vangl2*$^{m209/m209}$ embryo mosaically expressing Centrin-GFP, Membrane-GFP (green)
1324 and Par3-RFP (magenta). White arrows point at the BB at the beginning and at the
1325 end of the movie. Images were taken every 4 min during the 5 s to 6 s stages time-
1326 frame. Dorsal view. Corresponds to Fig7f.
1327
1328
1329
1330

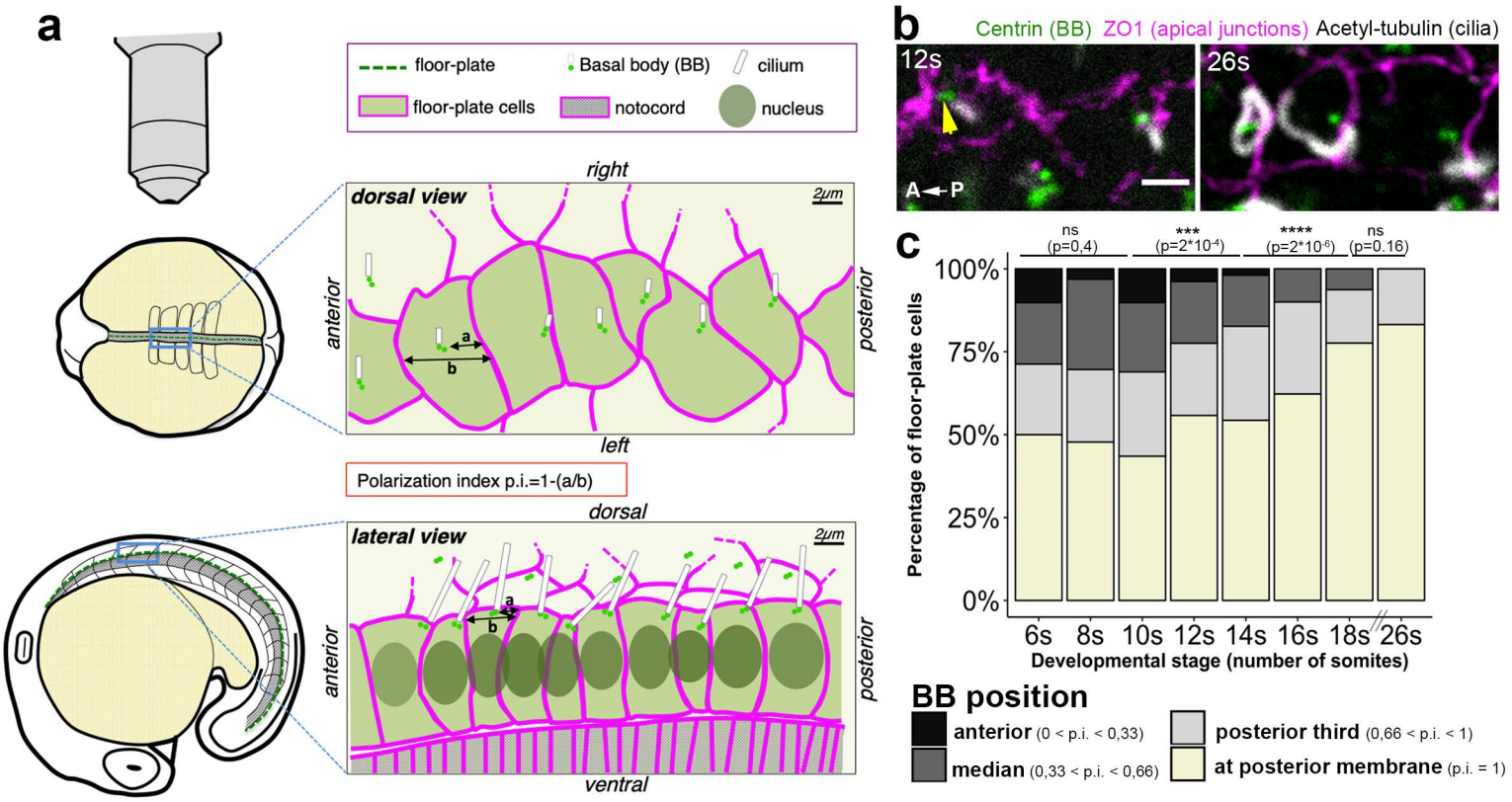

Figure1 Donati et al. 2020

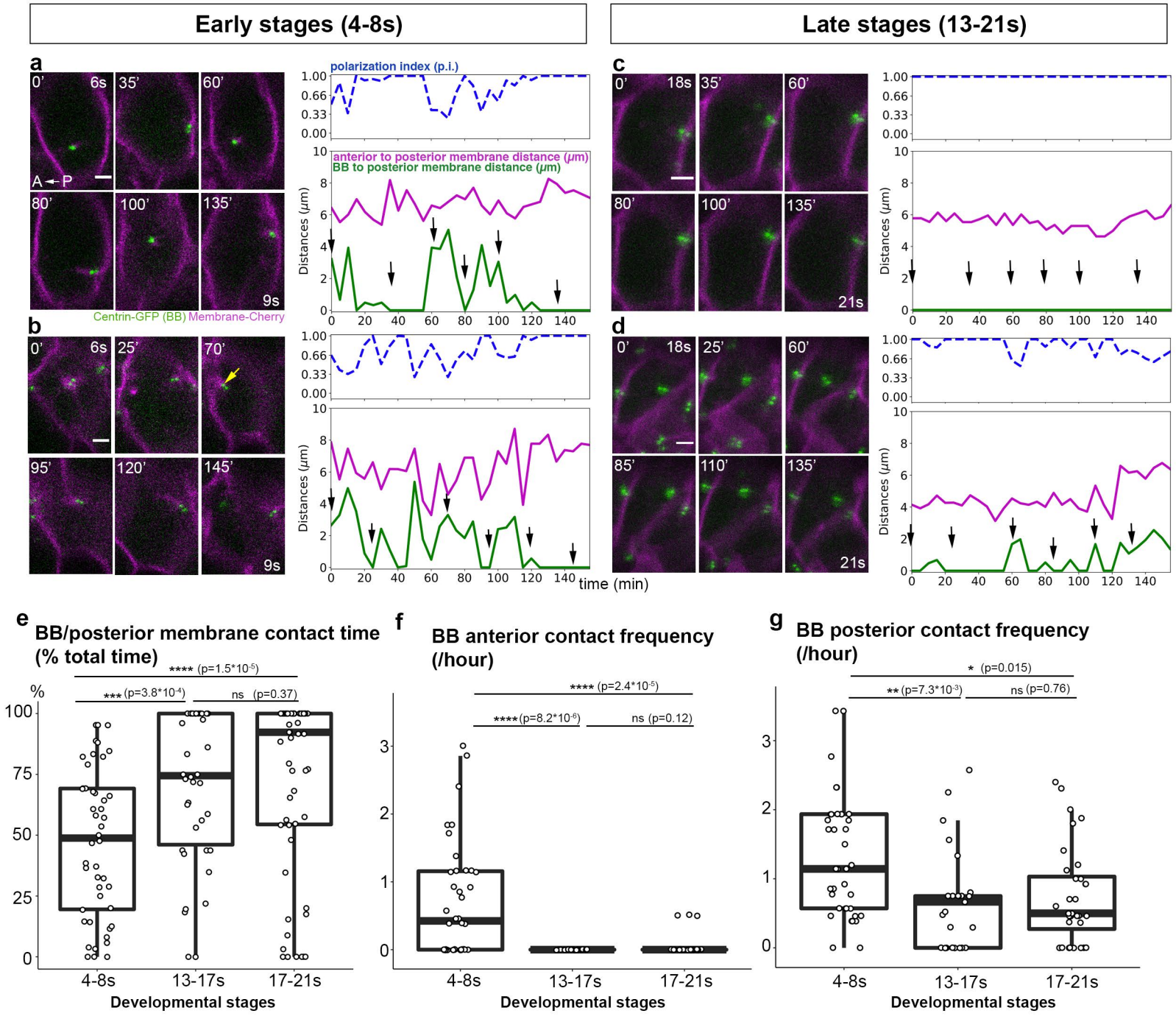

Figure2 Donati et al. 2020

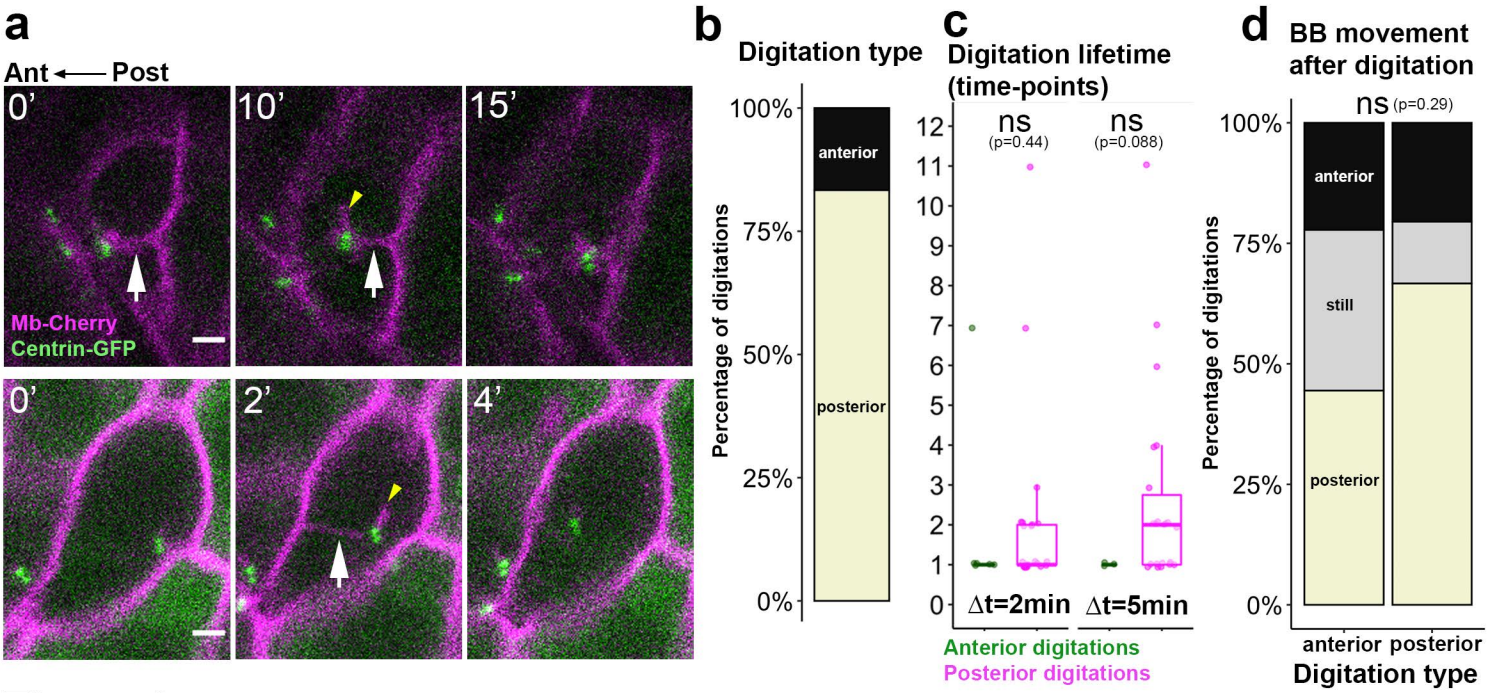

Figure3 Donati et al. 2020

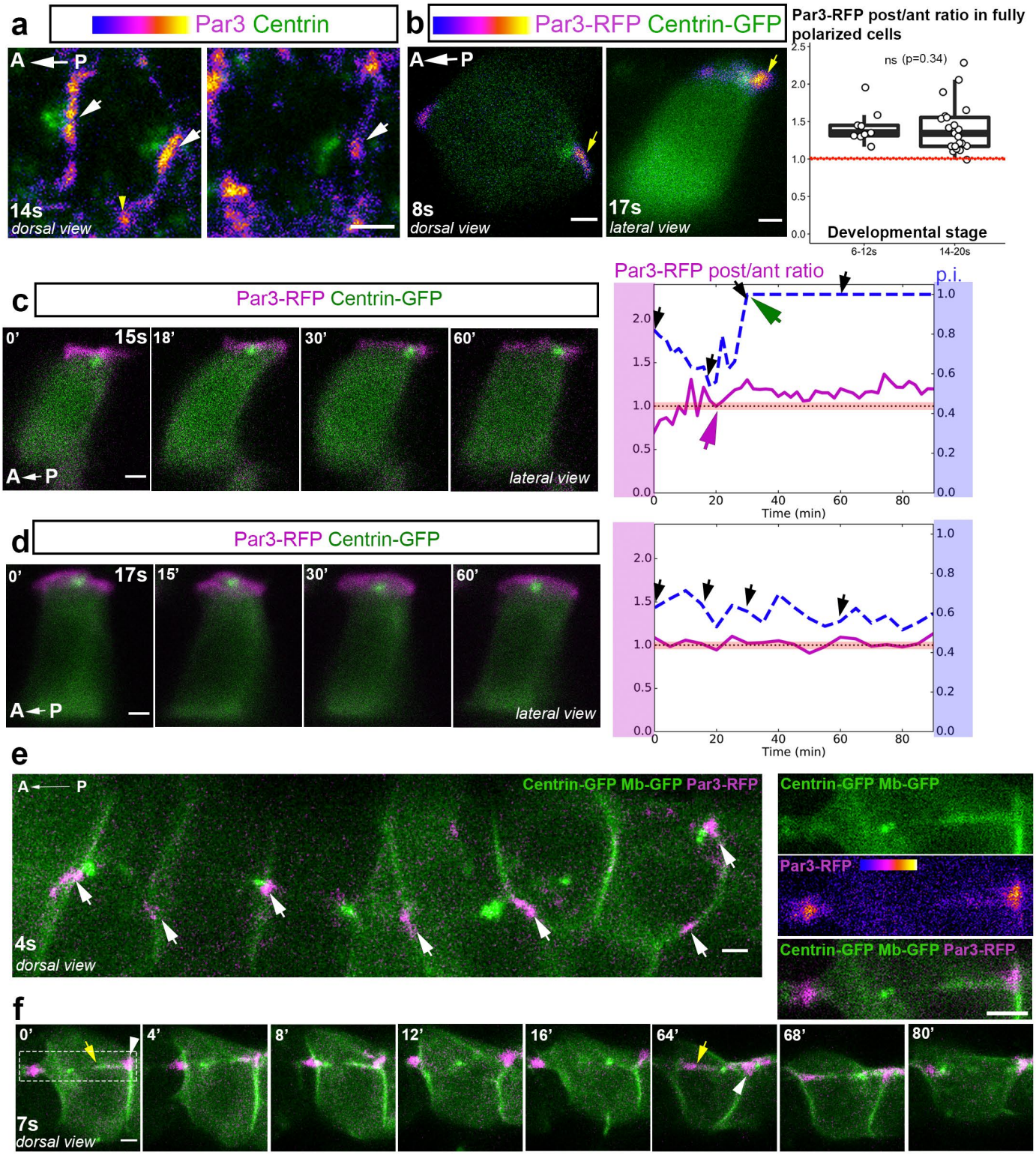

Figure4 Donati et al. 2020

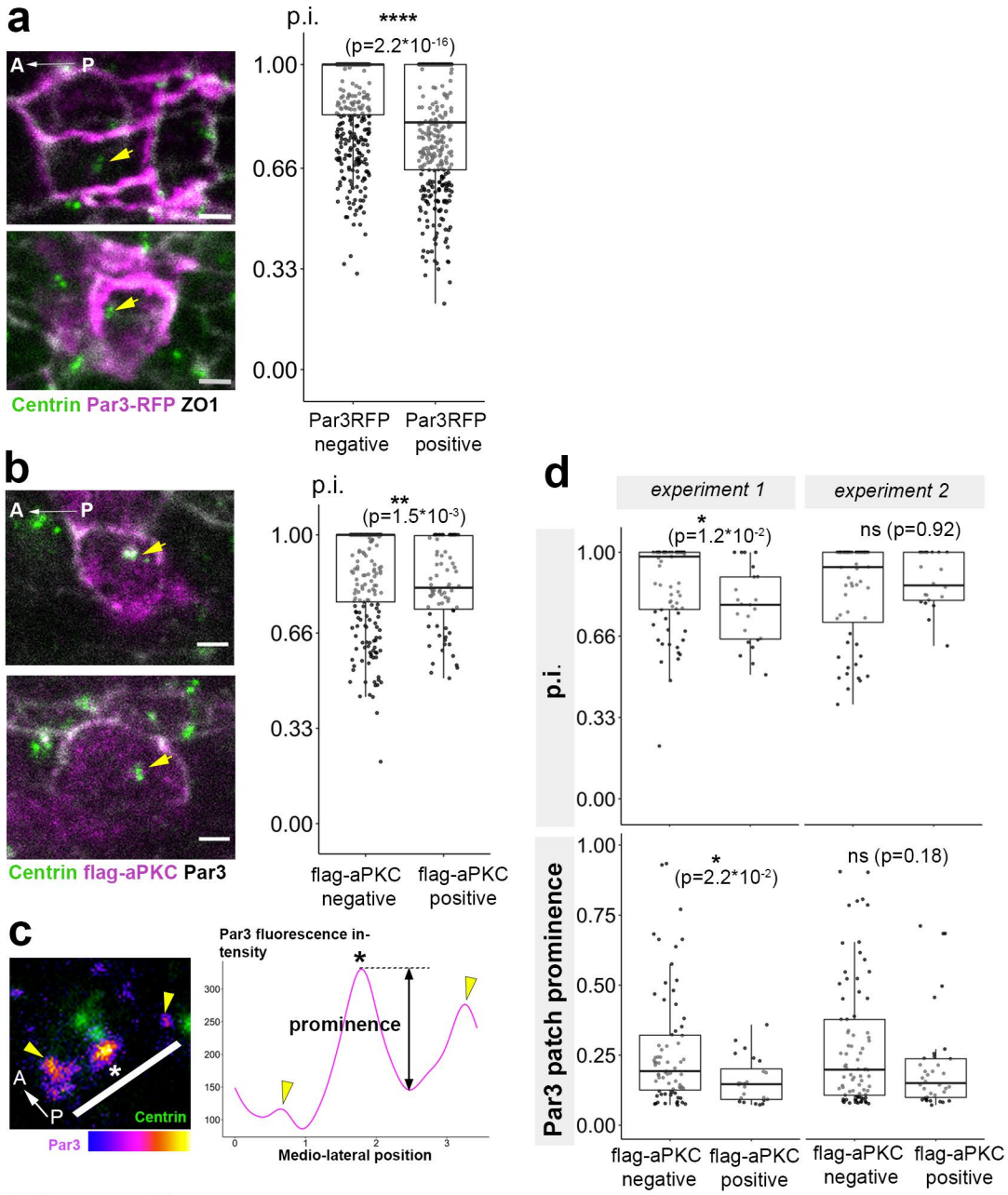

Figure5 Donati et al. 2020

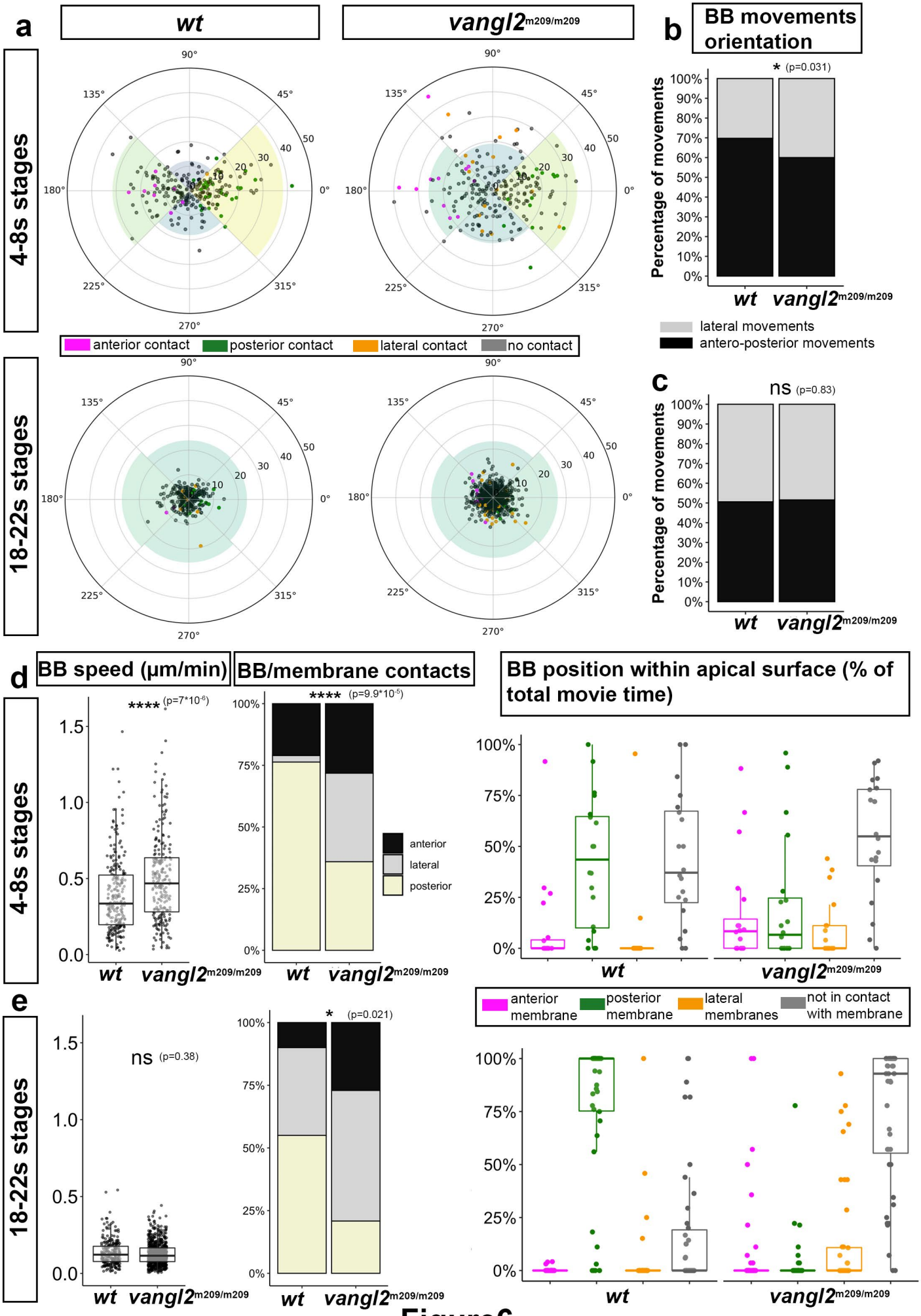

Figure6 Donati et al. 2020

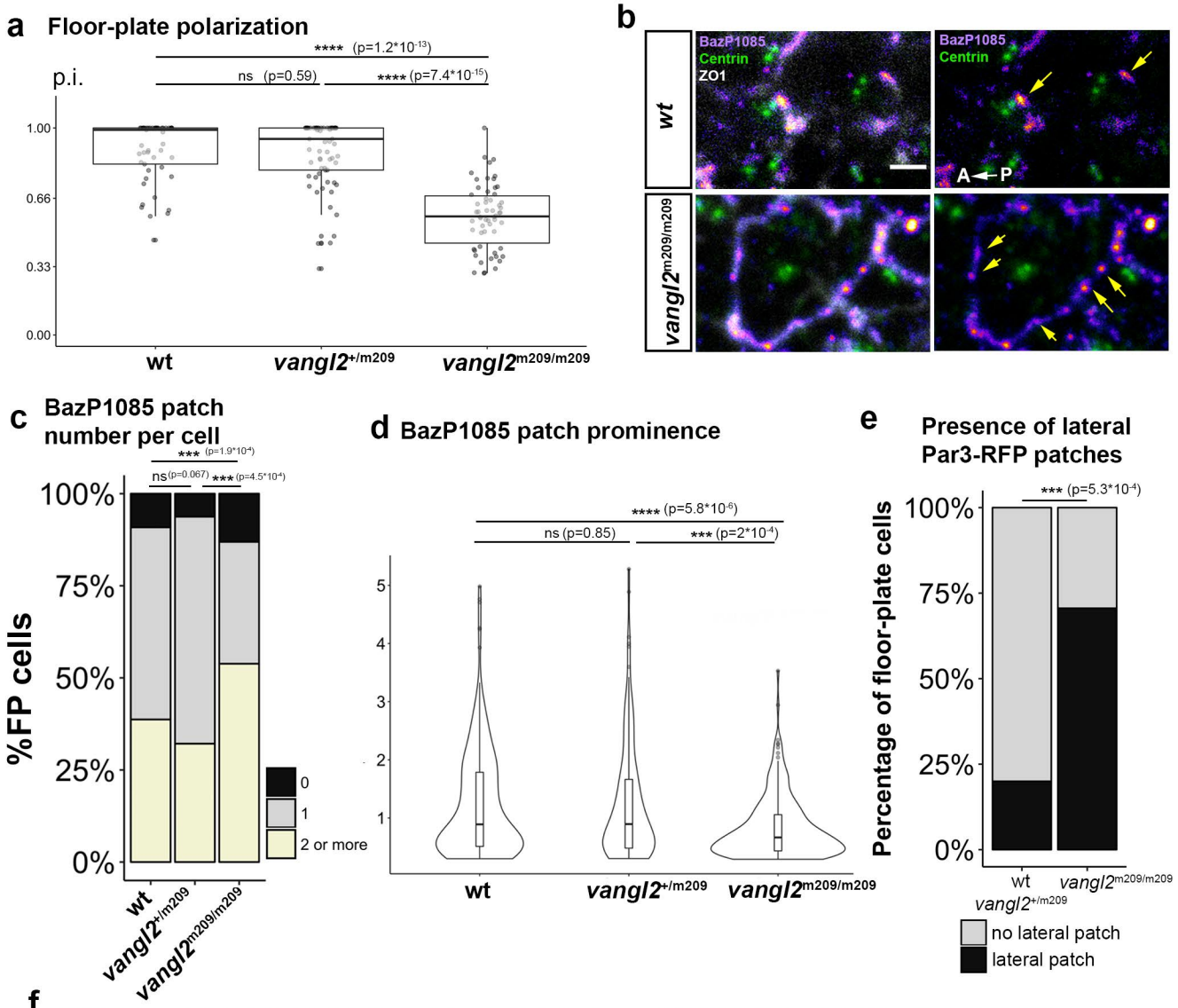

Figure7 Donati et al. 2020

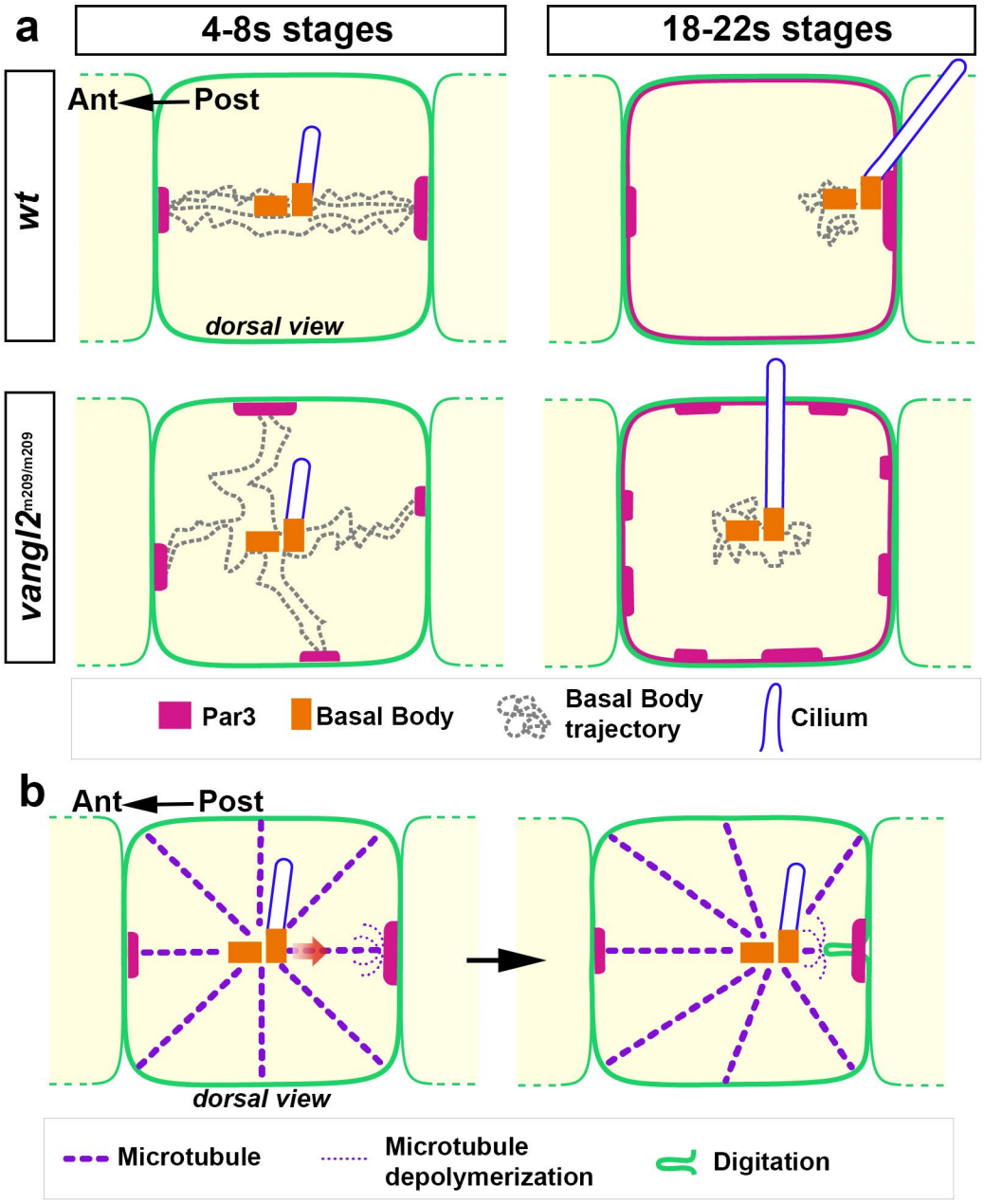

Figure8 Donati et al. 2020

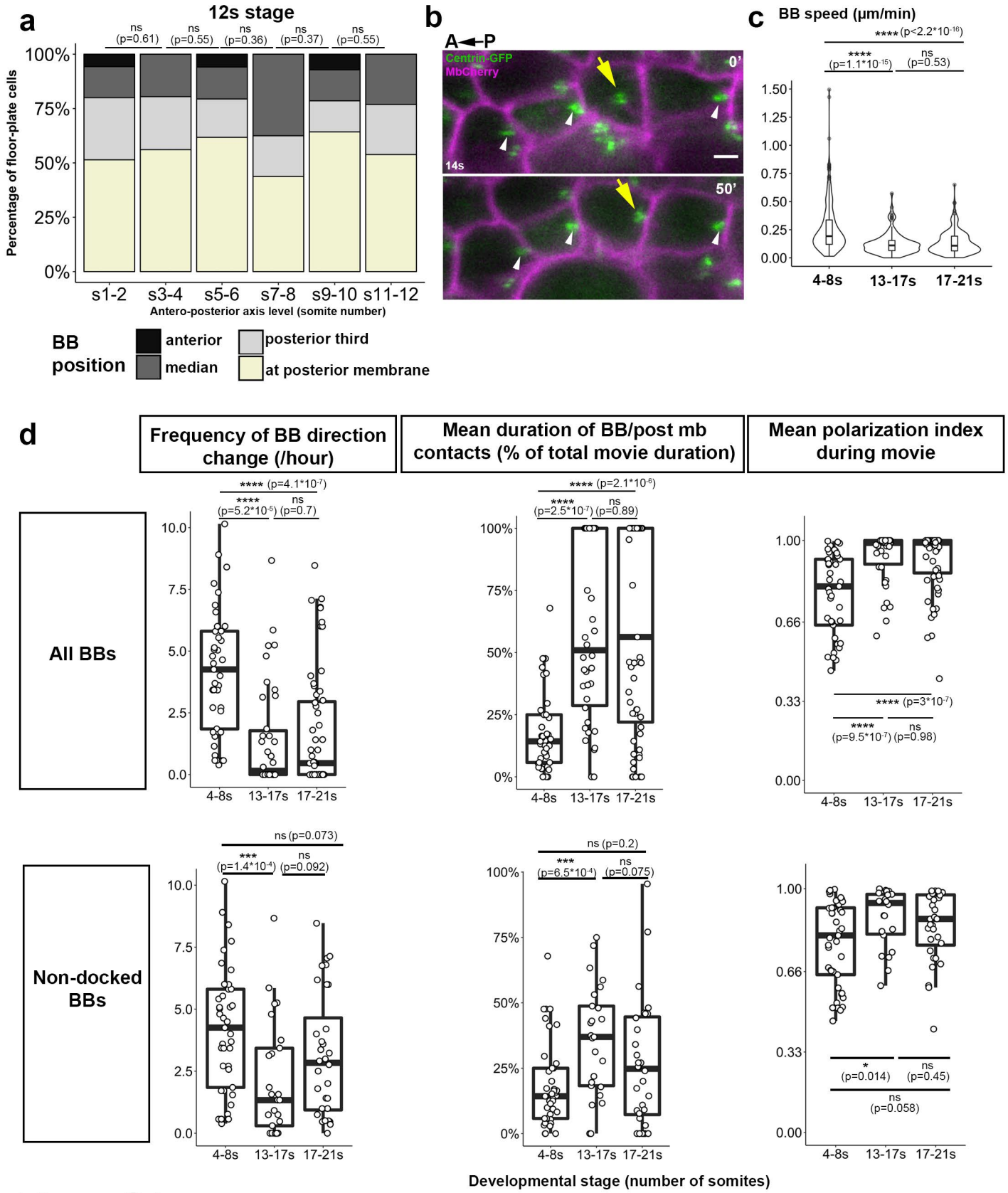

FigureS1 Donati et al. 2020

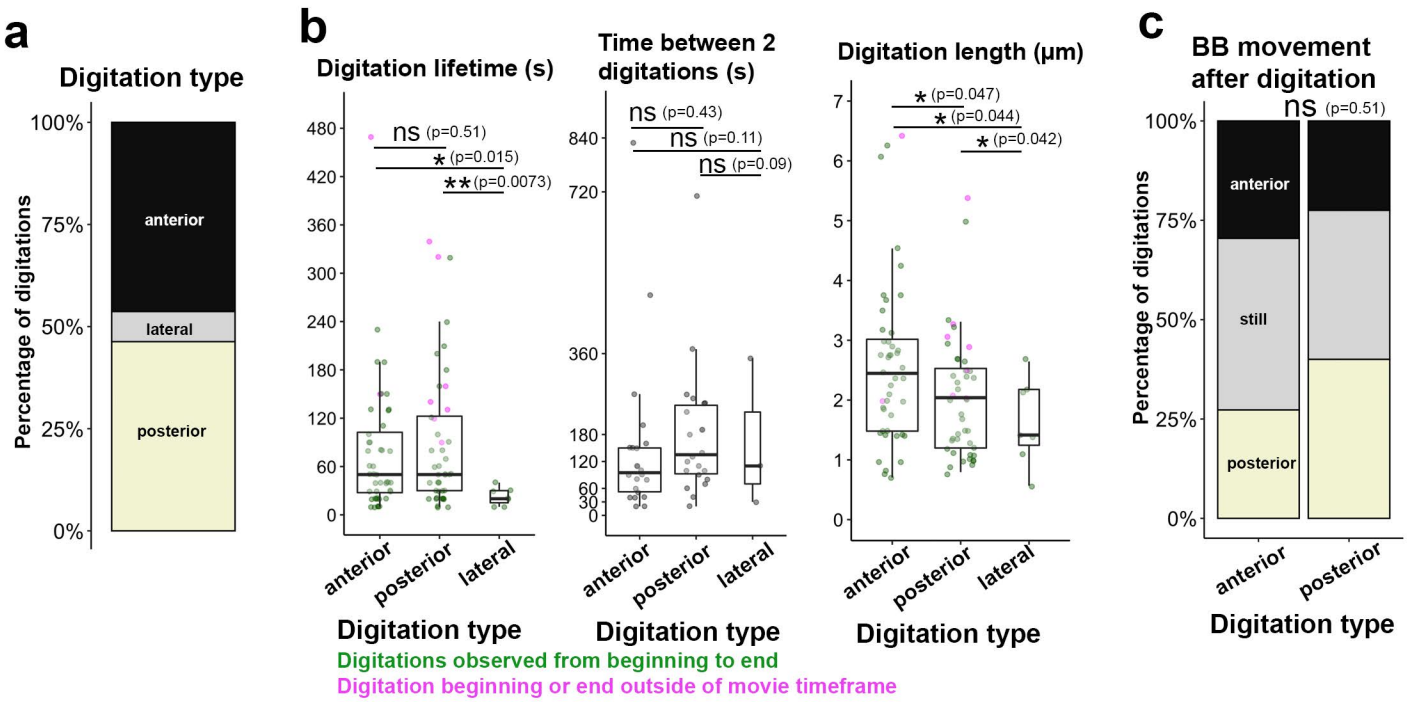

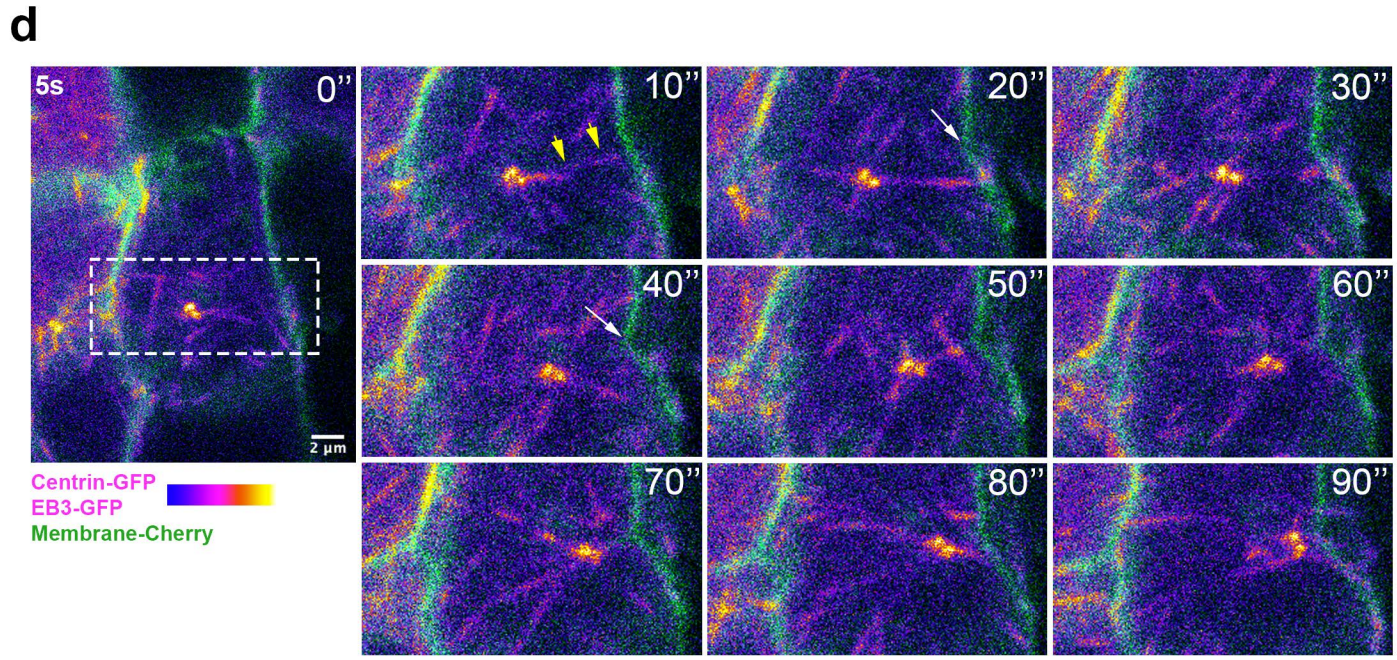

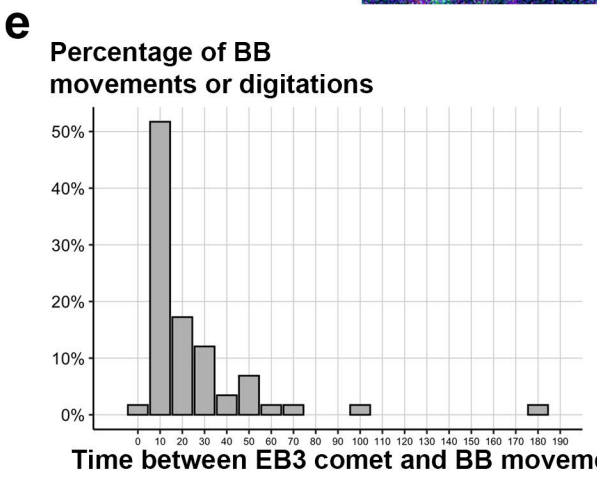

FigureS2 Donati et al. 2020

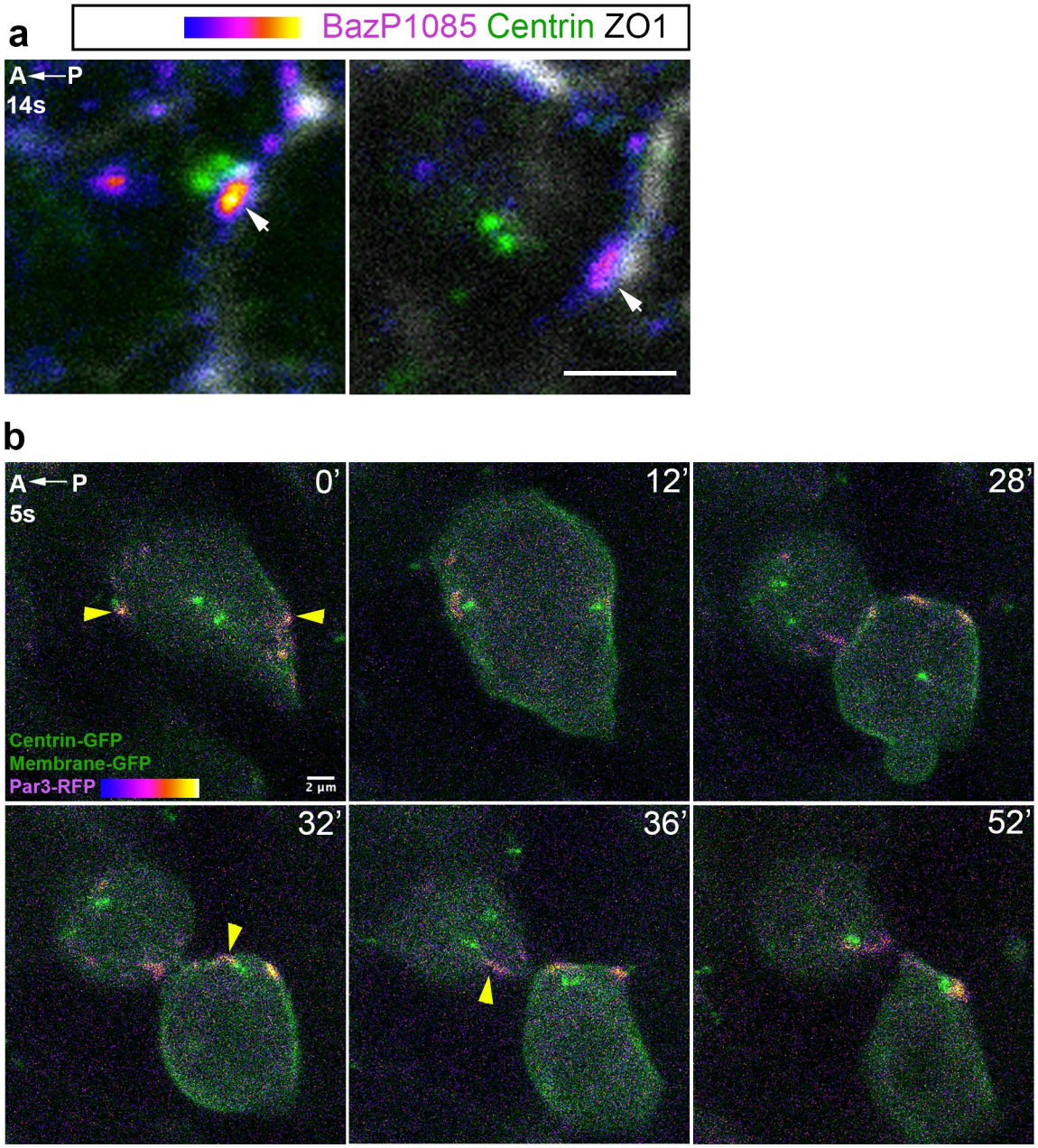

FigureS3 Donati et al. 2020

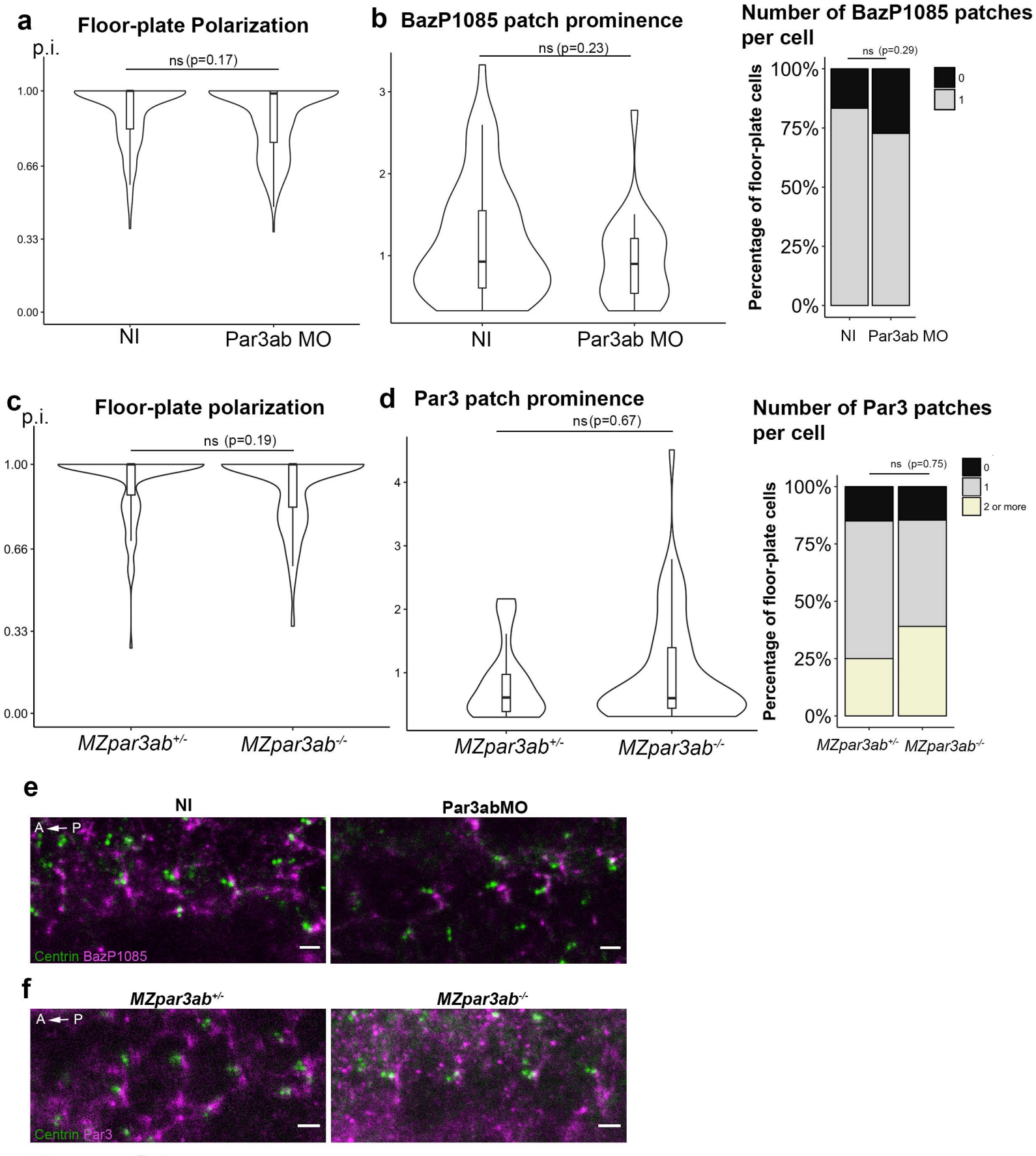

Figure S4 Donati et al.2020

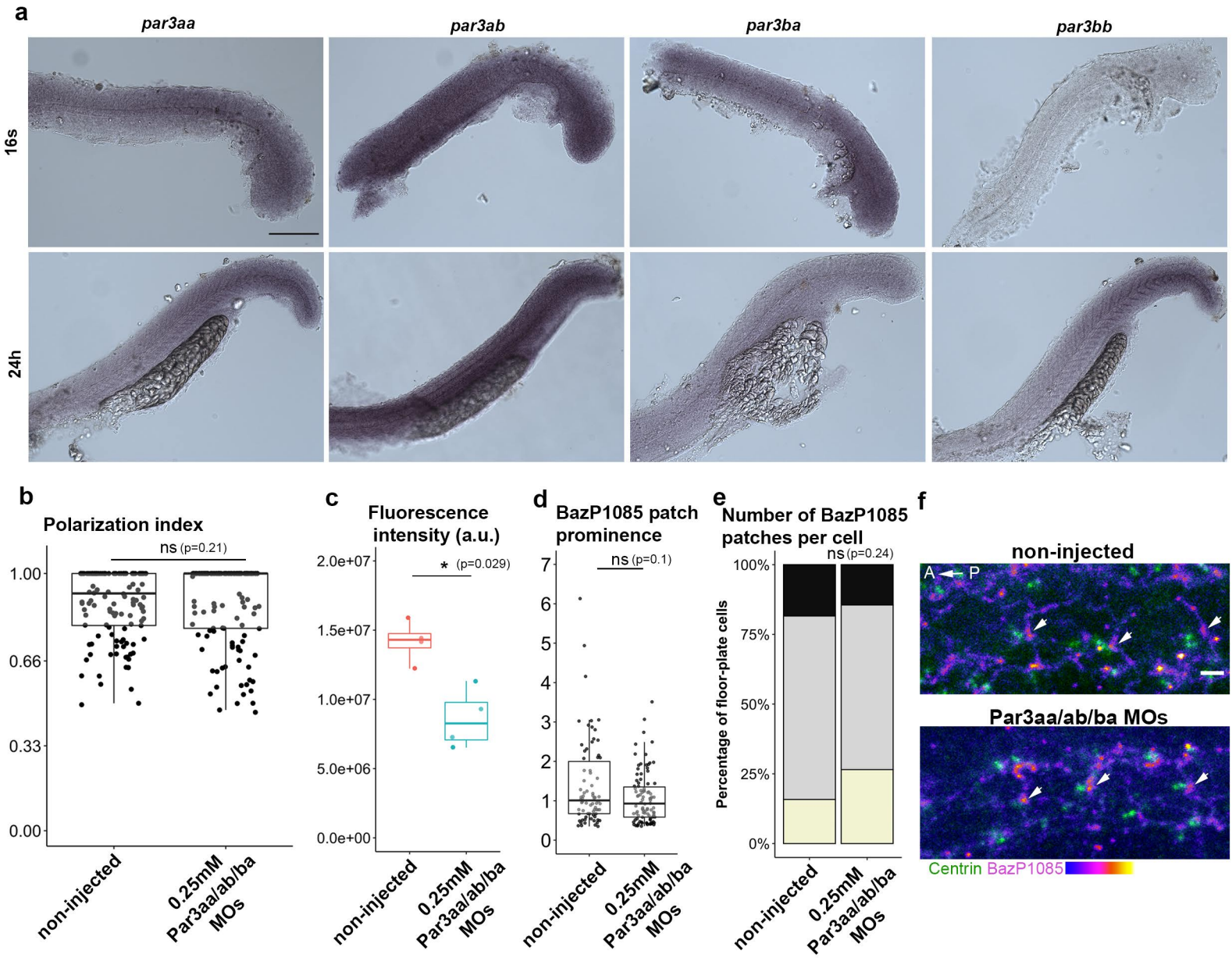

Figure S5 Donati et al. 2020